EUROPEAN ORGANIZATION FOR NUCLEAR RESEARCH

CERN-EP/87-102
3.6.1987

COLLINEAR FAST-BEAM LASER SPECTROSCOPY

R. Neugart

Institut für Physik
Universität Mainz
D-6500 Mainz, Fed. Rep. of Germany
and

the ISOLDE Collaboration, CERN, Geneva, Switzerland

Geneva, May 1987

To be published in:
Progress in Atomic Spectroscopy, Part D
Edited by H.-J. Beyer and H. Kleinpoppen
Plenum Press, New York

1. Introduction

The progress in atomic and molecular spectroscopy has gone hand in hand with improvements of the resolution. Before the tunable narrow-band lasers led to the invention of Doppler-free techniques, spectral lines from cooled hollow-cathode discharges[1] had typical widths larger than 300 MHz, and high resolution was achieved only in rf spectroscopy, e.g., within the hyperfine structure multiplets, by the classical techniques like atomic beam magnetic resonance[2], optical pumping[3] or double resonance[4]. While the Doppler broadening

$$\delta\nu_D = \nu_o \left(\frac{8kT\ \ln 2}{mc^2}\right)^{1/2} \tag{1}$$

is negligible for resonance frequencies ν_o in the rf regime, the narrowing of optical resonances by cooling to low temperatures, T, has obvious limits. On the other hand, eq. (1) holds for an isotropic thermal velocity distribution, and narrow Doppler width requires a reduction in the spread of velocity components only along the direction of observation. It is well known from ion optics that this can be achieved by electrostatic acceleration. If an ion beam propagates along the z direction, the constant phase-space volume requires that

$$\delta z\ \delta p_z = \text{const}, \tag{2}$$

and the broadening of the z distribution - due to acceleration - corresponds to a narrowing of the momentum distribution. Photons emitted along the beam have a considerably reduced Doppler width. This remained unobserved because of inefficient excitation mechanisms which cause intensity problems considering the extremely small solid angle required for the observation, and because of insufficient stability of the acceleration voltage.

With laser beams, the effect can be observed in absorption. This is the basis for collinear fast-beam laser spectroscopy. Among the Doppler-free techniques (described in Part A, Chapter 15 by W. Demtröder) it is the only one using linear absorption without velocity selection as in collimated atomic beams.

This offers the great advantage of optical resonance with the whole ensemble of atoms and yields an extremely high sensitivity, if the fluorescence is detected with a large solid angle. This advantage, and the fact that on-line isotope separators deliver many radioactive nuclides in the form of ion beams, have played the decisive role for the success of this technique in studies of atomic isotope shifts and hyperfine structures. On the other hand, the high-resolution spectroscopy on ions has been provided with a powerful experimental tool.

The roots of the experimental development can be traced back to the fast-ion-beam laser excitation performed by Andrä et al.[5], to measure lifetimes or quantum beats more precisely than by the unspecific beam-foil excitation (see Part B, Chapter 20). Here, the Doppler effect was exploited in tuning the laser frequency to an atomic resonance by a variation of the intersection angle between the ion and laser beams. The collinear or superimposed beam geometry was first used by Gaillard et al.[6]. Their Ba^+ beam from a standard 350-keV implantation unit had a large kinetic energy spread, and high resolution was achieved by probing the hole-burning effect of optical pumping with narrow-band laser light in a second interaction zone at a variable electrical potential. This elegant utilization of Doppler-tuning yielded the excited-state hyperfine structure in the $6s\ ^2S_{1/2} - 6p\ ^2P_{3/2}$ resonance line of Ba II[7] with a similar accuracy as the previous quantum beat experiments[8], but it avoided the need for high laser power and good spatial resolution in the differential detection along the beam.

Isotope shift and hyperfine structure studies on short-lived radioactive nuclides depend crucially on the sensitivity and the conditions of on-line production in nuclear reactions. Here, the search for a workable concept of experiments with fast isotope-separated beams was initiated by Otten. It was Kaufman who pointed out that the narrow velocity distribution along these beams corresponds to nearly Doppler-free conditions. The experimental scheme, worked out in early 1975[9], included cw-laser excitation with high resolution and efficiency of a neutralized fast

atomic beam and detection of the resonance fluorescence. A detailed discussion of the basic features[10] was followed by an experimental study on beams of the stable isotopes ^{23}Na and ^{133}Cs[11], and led to the wealth of new results on radioactive isotopes that will be discussed in Section 5.

However, the first experimental achievement of a narrow Doppler width in fast-beam spectroscopy was already reported independently by Wing et al.[12]. They performed the first precision measurements in the infrared vibrational-rotational spectrum of the simplest molecule HD^+ by crossing the ion beam with the beam from a single-mode CO laser at a very small intersection angle.

These pilote experiments were joined by the studies on the metastable Xe II, $5p^4 5d\ ^4D_{7/2}$ state in Xe^+ beams[13,14] from which the transition to $5p^4 6p\ ^4P_{5/2}$ is covered by the spectral range of the then standard laser dye Rhodamin 6G.

The present contribution complements several Chapters of the earlier volumes: it describes an additional technique of Doppler-free spectroscopy (Part A, Chapter 15 by W. Demtröder) for application with fast beams of ions or neutral atoms (Part B, Chapter 20 by H.J. Andrä) which has solved many problems of a systematic study of isotope shifts and hyperfine structures on short-lived nuclides (Part B, Chapter 17 by H.-J. Kluge). The need for a reliable isotope shift analysis adds weight to the discussion of Part A, Chapter 7 by K. Heilig and A. Steudel. The present Chapter will be devoted exclusively to the spectroscopy of atomic systems, i.e. neutral atoms and singly-charged ions, although the technique has many applications in molecular ion spectroscopy and reaction studies[15-21].

2. Basic Concept and Experimental Realization

The essential parameter for the resolution in fast-beam laser experiments is the kinetic energy spread of the ions. For low-energy beams ($E \lesssim 100$ keV) it is determined by the ion source and typically of the order 1 eV, if the acceleration voltage is well stabilized. To meet this value, plasma sources have to be operated with special care as for the pressure and potential distribution within the source. Surface ionization sources may almost reach the thermal energy spread of kT, but this requires very homogeneous and clean surfaces.

In estimating the velocity spread of an extracted beam, we assume an energy spread δE, not considering details of the distribution which strongly depend on the particular ion source. The dimensionless parameter $\beta = v/c$ is used for the velocity. For its dependence on the acceleration voltage U and the atomic mass m, it is sufficient to take the non-relativistic expression

$$\beta = \sqrt{2eU/mc^2} \quad . \tag{3}$$

The kinetic energy is $E = eU = \frac{1}{2} mc^2\beta^2$, and the conservation of the energy spread

$$\delta E = mc^2 \beta \delta\beta \tag{4}$$

involves a narrowing of the velocity distribution, proportional to the increase in the average velocity. The Doppler width is $\delta\nu_D = \nu_o \delta\beta$ for an optical frequency ν_o, and, using eqs. (3) and (4), we obtain

$$\delta\nu_D = \nu_o \delta E/\sqrt{2eUmc^2} \quad . \tag{5}$$

Here we have assumed a parallel beam for which the energy spread is transformed into a purely longitudinal spread of velocities. As an example, we obtain $\delta\nu_D = 5$ MHz for $\delta E = 1$ eV in a 50 keV beam of medium-mass ions ($A = 100$, $\beta = 10^{-3}$) and an optical frequency of 5×10^{14} Hz (6000 Å). This may be compared with the

natural line widths of strong atomic transitions which is of the order 10 MHz. That is to say, the homogeneous width matches the inhomogeneous Doppler broadening, and all atoms in the beam interact simultaneously with the laser light once the frequency is tuned to resonance. This gives the basic sensitivity for experiments with extremely low beam intensities, and in particular on the radioactive isotopes. If necessary, an additional homogeneous power broadening can be achieved quite easily.

In practice, one has to work with beams of a finite divergence depending on the emittance and the required beam diameter. For the present case, formula (73) of Part B, Chapter 20 by H.J. Andrä gives a vanishing contribution to the line width, because it includes only first-order terms in the angular dependence of the Doppler shift. For a symmetric full angular divergence $\delta\Theta$ around the beam axis ($\Theta = 0$) the additional broadening becomes $\nu_o \beta \, (1-\cos \frac{\delta\Theta}{2})$ or, using the lowest order term of the expansion,

$$\delta'\nu_D = \frac{1}{8} \nu_o \beta \, (\delta\Theta)^2 \, . \qquad (6)$$

In our example, for a beam divergence of 10 mrad, this gives an additional contribution of 6 MHz to the line width. It is thus obvious that the Doppler width in collinear geometry is rather insensitive to beam divergences. Correspondingly, the Doppler-shifted line positions are insensitive to small changes in the beam shape. This is a very important feature for Doppler-tuning experiments. For comparison, an intersection angle of 10° between the laser and the ion beam of the assumed divergence of 10 mrad would give a line width of almost 1 GHz, which means that high-resolution experiments of this type require more parallel and stable beams.

Of course, the superimposed-beam geometry involves a considerable Doppler shift of the transition frequency ν_o in the rest frame of the atoms. In the laboratory frame it is given by

$$\nu_{\pm} = \nu_o \frac{\sqrt{1 - \beta^2}}{1 \mp \beta} = \nu_o \frac{1 \pm \beta}{\sqrt{1 - \beta^2}} \qquad (7)$$

or, to first order,

$$\nu_{\pm} \approx \nu_o (1 \pm \beta) \qquad (8)$$

for parallel (+) or antiparallel (-) interaction, respectively. It is interesting noting that the velocity narrowing factor is proportional to the shift $\nu_o\beta$, or the product of Doppler width and Doppler shift is constant, namely $\nu_o^2\ \delta E/mc^2$. This shift requires a rather precise knowledge of the beam energy and the atomic mass for experiments in which frequencies in the atomic rest frame are to be determined. On the other hand, the Doppler shift offers great advantages: (i) Simple post-acceleration or deceleration can be used to tune the frequency seen by the fast moving ions. In our example of a 50 keV beam with $\beta = 10^{-3}$, the total Doppler shift is about 500 GHz, and a tuning range of 100 GHz is obtained with a ± 10 keV change in kinetic energy. (ii) As long as the atoms are ionized, the Doppler shift can be changed along the beam, and the interaction between the laser light and the ions can be switched on and of, or changed in frequency.

Still, many collinear fast-beam experiments have been performed on neutral atoms. For this purpose, the ions are neutralized by charge transfer, preferably in passing them through an alkali vapour cell. The charge-transfer cross-sections for the reaction

$$B^+ + A \rightarrow B + A^+ + \Delta E \quad ,$$

where B^+ represents the fast ion and A the alkali atom, are generally of the order 10^{-15} to 10^{-14} cm^2 and particularly large, if the energy defect ΔE is small (near-resonant electron transfer)[22-25]. These collisions occur with negligible energy transfer of the order $(\Delta E)^2/eU$ to the target atoms, and therefore the velocity distribution in the neutralized beam remains nearly unchanged. This also means that all arguments and estimates for the resolution and sensitivity remain valid.

Moreover, the missing energy ΔE is converted completely into additional kinetic energy of the fast beam. If several states of the atom B are populated in the electron capture, the beam is composed of atoms with several discrete velocities which can be observed in the Doppler-shifted optical resonances[11]. These velocity spectra give a direct access to the final-state distribution of the charge transfer process, provided that the atoms decay rapidly into the ground state from which they are excited by the laser light. The components are well-resolved only for beam energies up to a few keV, where the change in the Doppler shift for a separation of a few eV is still larger than the natural linewidth. At higher beam energies, the effect may contribute to an additional line broadening.

If metastable states are among those favoured by the resonance condition $\Delta E \approx 0$, the neutral beam contains a large fraction of metastable atoms. This gives an access to transitions which are difficult to observe otherwise. It is a particularly important feature that many elements with high excitation energies, or UV resonance lines from the ground state, have metastable states with binding energies close to the ground state of the alkali atoms between - 4 and - 6 eV. The selective population of these states can be controlled by the choice of the alkali vapour target (Na: - 5.1 eV, Cs: - 3.9 eV) and the optical excitation can be induced by cw laser light in the visible[26,27]. Such procedures have contributed a lot to the versatility of the technique and they have been used extensively in the isotope shift and hyperfine structure studies on long sequences of unstable isotopes[27] (See Section 5).

Although the details of the experimental set-up have to be taylored for the special purpose, we have a simple basic design which is slightly different for spectroscopy on ions and neutral atoms. This is outlined in Fig. 1. The ion beams may be provided by any source which has a low energy spread, and accelerated by a sufficiently stable voltage (typically between 1 and 100 kV). For ion spectroscopy (a), this beam,

merged with the laser beam, is transmitted through the observation chamber which forms a Faraday cage at a variable potential. The set-up for neutral atoms (b) includes a charge-exchange cell[28,29] in which the alkali vapour pressure of about 10^{-3} torr is maintained by heating. The Doppler-tuning potential is applied to this cell and the observation chamber has to be put as close as possible to avoid optical pumping to non-absorbing states.

Omitted in Fig. 1 is all ion optics, and in particular the deflection into the laser beam axis, except for the acceleration/deceleration system in front of the observation chamber or charge-exchange cell. The latter has to minimize lens and steering effects of the tuning potential. It usually consists of a set of cylindrical electrodes which produce a smoothly varying potential along the beam axis.

The collection of fluorescence photons can be performed by lenses, mirrors, light pipes, or a combination of them, and the design has to be optimized for the special conditions of the experiment. In particular, if the atomic spectrum excludes the rejection of laser light background by optical filters, one has to find a compromise between large solid angle and low acceptance for the scattered light.

A few examples of the practical versions of this basic set-up will be given in the review of experiments. Most of them use clean mass-separated beams, although the laser-induced fluorescence is selective for the element and the resonances of different isotopes are well separated by the Doppler effect.

3. Experiments Based on the Doppler Effect

The considerable Doppler shift in all collinear-beam experiments has opened up a few general applications beyond the spectroscopy of particular atomic or molecular systems. The scope of such applications ranges from simple beam velocity analyses to precision experiments related to metrology or fundamental physics problems. These latter include the calibration of high voltages and measurements of the relativistic Doppler effect, for which the atomic transition frequency provides an intrinsic clock.

3.1 Beam Velocity Analysis

The measurement of the velocity distribution in (low-energy) ion beams is conventionally performed using electrostatic analyzers or the time-of-flight technique which also works with neutral beams. As the time of flight the Doppler shift essentially measures the beam velocity v. However, the measured time interval decreases, whereas the Doppler shift increases proportionally with v. This gives decisive advantages of the Doppler shift technique for higher beam energies.

A more quantitative comparison is easily performed by use of eq. (4). We assume that a fixed time interval δt can be resolved at the detector placed at a distance L from the chopper slit. Sufficiently fast choppers consist of electric deflection plates for the initial ion beam and a slit defining the entrance of the drift space, e.g. after a collision chamber where neutral products may arise from specific reactions. Then the energy resolution is given by

$$\delta E = \frac{(2E)^{3/2}}{m^{1/2}} \frac{\delta t}{L} \quad . \tag{9}$$

If the chopper instead of the detector determines the time resolution, it can be shown[30] that for optimized electric field amplitude of the deflector

$$\delta E = 2\sqrt{2}\, E \frac{s}{(DL)^{1/2}} \quad , \tag{10}$$

where s is the width of the slit and D the distance of the deflector from the slit. A practical example for helium and L = 2.5 m is given in ref. (30). For δt = 7.5 ns, δE is increasing from 1 eV to 7 eV for beam energies E between 800 eV and 3 keV. This is well consistent with eq. (9).

For the Doppler shift measurement we obtain

$$\delta E = (2Emc^2)^{1/2} \quad \frac{\delta\nu_o}{\nu_o} \tag{11}$$

where $\delta\nu_o$ is the natural (or power-broadened) line width of the transition involved. For the quoted example this would give $\delta E \approx 0.1$ eV, if the atoms could be excited by an optical transition of typically $\delta\nu_o/\nu_o = 4\times10^{-8}$. This is possible only for the metastable 1s2s states, whereas the helium atoms in the ground state are inaccessible, because their resonance absorption lies in the far UV. We note here a general difference of both techniques: The time-of-flight spectra include all atoms in the beam, while the optical spectra only show the part of the atoms which are in the absorbing level. Therefore, apart from energy resolution arguments, both methods can be complementary to each other.

Coming back to our comparison we find that beyond mass A ≈ 40 (with all other parameters unchanged) the time-of-flight resolution will become superior to the optical. But the energy dependence shows that for beam energies above a few keV the Doppler shift measurement becomes definitely more favourable. Moreover, the choice of a weak transition with small natural line width can give another gain in resolution at the expense of fluorescence intensity. The basic resolution can be exploited in studies of the primary beam velocity distribution from the ion source. Fluctuations arising from instabilities of the acceleration voltage or the plasma potential may be eliminated by regulating the velocity with the Doppler-tuned resonance signal. This was demonstrated by Koch[31] who excited a neutralized ^{4}He beam containing 1s10p Rydberg atoms to a higher

Rydberg level by a CO_2-laser line and used the ionization in a microwave cavity to produce the reference signal.

In studies of secondary collision processes and their energy-loss spectra, it is clear that the resolution is limited by the energy spread of the original ion beam. An example[32] is given in Fig. 2 which shows the energy-loss spectrum of the charge transfer from a 7 keV Cs^+ beam to Cs vapour, on top of the hyperfine structure of the transition $6s\ ^2S_{1/2} - 7p\ ^2P_{3/2}$ at 4555 Å. The energy resolution of 0.7 eV is mainly determined by the ion source. The small satellite peaks at low vapour pressure are due to the non-resonant channel

$$Cs^+ + Cs(6s) \rightarrow Cs(6p) + Cs^+ - 1.4\ eV.$$

With increasing vapour pressure these peaks become stronger, and additional equidistant peaks become observable. This is ascribed to secondary excitations, according to

$$Cs(6s) + Cs(6s) \rightarrow Cs(6p) + Cs(6s) - 1.4\ eV.$$

From such a sequence of curves, one can extract the branching ratio of the primary electron capture into 6s and 6p, as well as the cross-section for collisional excitation in the fast atomic beam. Similar examples of state-resolved charge transfer are given in ref. (11) for Na^+ on Na and K and in ref. (27) for Yb^+ on Na. The time-of-flight technique, on the other hand, has yielded the metastable composition of a $2\ ^3S$ He beam formed by charge exchange on alkali atoms[33].

3.2 High Voltage Measurement and Calibration

So far we have disregarded the excellent internal velocity calibration which is provided by a measurement of the laser frequency. It can be helpful for precision spectroscopy experiments, but also used to calibrate voltages beyond a few keV with unprecedented accuracy. Voltages up to a few hundred keV are measured by compensated dividers, consisting of wire

resistors, with relative uncertainties down to 3×10^{-5}. Commercial instruments reach the 1×10^{-4} level.

In this context there have been two approaches of absolute beam energy measurement, (i) by accurate measurements of the Doppler-shifted resonance frequencies (or wavelengths) with parallel and antiparallel beams, and (ii) by using two-photon interactions of a three-level system in counter-propagating laser fields. As atomic masses are known very precisely, we do not differenciate between velocity and kinetic energy.

(1) The straightforward solution simply consists in a measurement of the Doppler shift. The limited use of fixed-frequency lasers with known wavelength has been circumvented by the choice of IR transitions between Rydberg states of which the lower is populated in a charge-transfer reaction[31]. Still, this gives rather poor accuracy, even if both the laser and the Rydberg transition frequencies are known precisely. Optical transition frequencies from tunable dye lasers can be measured to about 10^{-8} using fringe-counting wavemeters [34,35] calibrated against an I_2-stabilized HeNe laser. This precision corresponds roughly to the line widths of both the laser and the atomic transition. From a measurement of the Doppler-shifted resonance excitation frequencies for parallel and anti-parallel laser and atomic beams it follows from eq. (7) that the beam velocity

$$\beta = \frac{\nu_+ - \nu_-}{\nu_+ + \nu_-} \qquad (12)$$

is determined by the two wave numbers ν_+ and ν_-. Assuming a sufficiently mono-energetic beam one obtains an accuracy $\delta\beta = \frac{1}{\sqrt{2}} \delta\nu/\nu_o$, independent of β. Since the relative accuracy increases with β, one should use light atoms. Here, the outstanding example for laser spectroscopy is the Balmer-α line of atomic hydrogen. In a pilote study[26] the metastable 2s state was populated by near-resonant charge transfer with cesium, and the Balmer-α excitation was detected as a flop-out signal in the Lyman-α radiation induced by an electric quenching

field. For a 7.5 keV deuterium beam the width of the laser-induced resonance 2s-3p was 234 MHz, due to the 2.3 V energy spread of the ion source and the hyperfine structure. This modest resolution already corresponds to an energy determination to 2×10^{-5}, if one assumes that the line centers can be determined within 10 % of the width. As the natural line width is 29 MHz, a considerable gain in resolution is expected[36] from the installation of an electrostatic velocity filter which can supply beams of $\delta E = 50$ meV. With a resolved hyperfine structure, such a set-up should reach a 1×10^{-6} uncertainty in the beam energy. The precision may also be interesting for a redetermination of the Rydberg constant of which the latest values are given with an error of 1×10^{-9} [37,38].

(ii) An alternative possibility to determine beam energies[39] is based exclusively on atomic transition frequencies and special features of a particular atomic level scheme. The simultaneous resonance of the fast atoms with the direct and retro-reflected laser light on two different transitions (resonant two-photon absorption, V or Λ configuration) determines the velocity to

$$\beta = \frac{\nu_2 - \nu_1}{\nu_2 + \nu_1} \quad , \tag{13}$$

where ν_1 and ν_2 are the transition frequencies in the rest frame of the atoms. Small detunings from the simultaneous resonance can be measured sufficiently accurate in laser or voltage scans and used to correct formula (13). However, most of the atomic transition frequencies have to be known more precisely than tabulated. They can be improved by new laser measurements. A more decisive drawback of this technique is the small voltage range covered by a specific atomic level scheme. Poulsen[39] gives a list of candidates for calibration points over a large energy range, from 50 keV up to several MeV. At such high energies the disadvantage of heavier atomic systems (ranging from Ne to U) is unimportant for the relative precision. An advantage is the possibility to set up secondary voltage standards based exclusively on atomic parameters.

The high precision of beam energy measurements does not necessarily correspond to a high precision of the voltages. This requires also a detailed knowledge of the ion source parameters, and in particular the ion formation at a well-defined potential. With some precaution, a conversion from the energy to the voltage scale should be possible within less than 1 eV, whereas for higher absolute precision one has to avoid or compensate carefully any contact potentials.

3.3 Relativistic Doppler Shift

The measurement of absolute beam velocities, or the calibration of voltages is already quite sensitive to the relativistic quadratic term in the Doppler shift formula (7). In fact, this "transverse" Doppler shift, caused by the time-dilatation factor $\gamma = (1-\beta^2)^{-1/2}$ was first observed in the spectral lines of fast moving hydrogen atoms from a 30 keV beam of H_2^+ ions, viewed along and opposite the direction of propagation[40,41]. Comparable accuracy in the percent range was also achieved in Mössbauer experiments[42], and more recently the time dilatation factor on the muon lifetime was determined to 1×10^{-3} [43].

New laser experiments with fast atomic beams could simply measure the resonance frequencies in the laboratory frame

$$\nu_{\pm} = \nu_o \gamma(1 \pm \beta) \tag{14}$$

for parallel and antiparallel beam-laser interaction, which gives

$$\nu_+ + \nu_- = 2\nu_o \gamma \tag{15a}$$

$$\nu_+ - \nu_- = 2\nu_o \gamma\beta \ . \tag{15b}$$

For H_α spectroscopy ($\nu_o = 4.57 \times 10^{14}$ Hz) on a 100 keV hydrogen beam ($\beta = 1.5\times10^{-2}$) one could imagine an uncertainty of the order 10^{-4} in the second-order shift of 50 GHz ($\gamma-1 \approx \frac{1}{2}\beta^2 = 1.1\times10^{-4}$) from a state-of-the-art wavemeter[34,35,44]. However,

this contribution appears on top of a huge first-order shift, which makes the measurement extremely sensitive to beam energy fluctuations. Nevertheless, Juncar et al.[45] have shown that an accuracy comparable to the best previous experiments can be achieved with moderate experimental effort. An alternative is the elimination of the first-order shift which also helps to avoid the clumsy measurement of absolute wavelengths for the determination of a relatively small difference. Such an alternative was already sought in the first-generation laser experiment by Snyder and Hall[46]. A beam of fast neon atoms in the metastable 3s $[3/2]_2$ state was transversely excited to 3p' $[1/2]_1$ in a standing-wave laser field. The saturation peaks, observed in fluorescence, are free from first-order shifts, provided that the optical alignment is perfect. Even a small deviation 2α from perfect retro-reflection introduces a significant residual first order-shift $\nu_o \alpha\beta$. Therefore, an improvement in the transverse shift far beyond the reported 6×10^{-3} appears very difficult.

The advantages of collinear geometry and a purely relativistic Doppler effect can be combined in a resonant two-photon absorption experiment[47]. The two photons are absorbed from the direct and the retro-reflected laser beam of frequency ν_L, and a few atomic systems[47,39] have intermediate states that can be tuned into resonance at a beam velocity selected by

$$\nu_1 = \nu_L \quad \gamma(1+\beta) \tag{16a}$$

$$\nu_2 = \nu_L \quad \gamma(1-\beta) \tag{16b}$$

where ν_1 and ν_2 are the frequencies connecting the intermediate level with the lower and upper ones. Fig. 3, taken from Poulsen and Winstrup[47], shows such an example in the energy-level diagram of NeI and Fig. 4 compares the narrow two-photon resonance in a laser-frequency scan with the broad detuning curve for the intermediate level in a voltage scan. The width of 4.7 MHz for the two-photon resonance is mainly composed of

the laser bandwidth, second-order Doppler broadening, the natural width of the upper level and some power broadening. Poulsen and Winstrup also demonstrate that the ac Stark shift vanishes at resonance, which is in accordance with theoretical predictions[48].

A recent upgraded version[49] of this experiment led to a new precision measurement of the relativistic Doppler shift in a 120 keV neon beam. The resonantly enhanced two-photon absorption in the beam was compared with the non-resonant two-photon absorption of neon atoms in a low-pressure discharge cell. With the very precisely known transition frequencies ν_1 and ν_2[44] there was no need to measure the beam velocity: The two-photon resonances in the cell at $\nu_C = (\nu_1 + \nu_2)/2$ and in the beam at $\nu_B \simeq \sqrt{\nu_1\nu_2} = \gamma\nu_C$ were induced by two frequency-stabilized laser beams whose beat frequency of about 3 GHz was measured on a fast photodiode. This gives the experimental Doppler shift of 3235.94(14) MHz in excellent agreement with the prediction 3235.89(5) MHz of special relativity. All possible error contributions are considerably smaller than the statistical error of 0.11 MHz for the beat frequency, obtained with a width of 3 MHz (FWHM) for both resonances and extrapolation to zero of the neon pressure in the cell. In particular, the errors for a slight angular misalignment Θ give negligible frequency shifts of the order $\nu_o\beta\Theta^2$. A significant improvement over the present accuracy of 4×10^{-5} would require higher-energy beams of excellent velocity stability and better absolute values of the transition frequencies.

4. Spectroscopic Studies

Many of the spectroscopic studies were performed to demonstrate the capability of the technique and a number of variants which are specific for the combination of laser spectroscopy with fast beams of ions or atoms. An example has already been discussed in Section 3.3: Resonant two-photon excitation becomes possible by adjusting the Doppler shifts for interaction with the direct and retro-reflected laser beam to the atomic transition energies. Other features include the preparation of otherwise unaccessible atomic states, the separation of hyperfine structures from different isotopes by the Doppler shift, or the observation of time-resolved transient phenomena along the beam. The extensive research on nuclear moments and radii from the hyperfine structure and isotope shift constitues a self-contained programme which will be discussed separately in Section 5.

The experiments are not discussed systematically, as their scope ranges from the development of the instrumentation to the study of particular atomic systems. This indicates that during the first decade the technique has provided a playground for the experimentalist rather than established a standard procedure of atomic structure studies.

4.1 Experimental Details

Many experiments were performed with a set-up which is similar to the one outlined in Fig. 1. The beam energy ranges from 1 to 200 keV, sometimes given by the particular lay-out of an existing machine or isotope separator. As the essential parameters like Doppler shift and narrowing as well as the charge-transfer cross-sections depend on the ion velocity, the choice of the beam energy is not very critical for most applications. Generally, the Doppler broadening from the ion source energy spread drops with increasing beam energy, while the stability and precision measurement of the acceleration voltage becomes more important. The charge-transfer neutrali-

zation at higher beam energies gives a broader distribution over the final states with decreasing total cross-sections only for the near-resonant cases[22-25]. On the other hand, the broader energy spectrum of the neutral products is again compensated by the improved narrowing.

Surface ion sources are used for elements with ionization energies up to 6 eV. With clean surfaces they give beams of small energy spread and a well-defined starting potential for the ions. ($\delta E < 0.5$ eV were achieved for Rb^+ and Cs^+ from a tungsten surface[50,51].) Various types of discharge ion sources have been used for elements with higher ionization energy. Their energy spread depends crucially on the operating conditions and can be reduced to a few eV for most standard-type sources, by minimizing the potential gradient over the effective source volume. In general, the optical line widths lie between 10 and 100 MHz, and only for very light elements or narrow lines the residual Doppler width is an important drawback for the resolution.

A calibration problem for Doppler tuning arises from the poorly defined absolute beam energy, due to the potential of the plasma surface. Several techniques have been applied to circumvent this problem: (i) A calibrated laser-frequency scan is used to compensate a certain Doppler detuning of the resonance, and with known $\Delta\nu$ and ΔU the unknown beam energy eU - in first-order approximation

$$eU = \frac{e^2}{2mc^2} \nu \frac{\Delta U}{\Delta \nu} \qquad (17)$$

- can be eliminated[52]. (ii) The absolute Doppler shift can be measured by comparison with the atlas of the I_2 or Te_2 absorption spectra[53] or by a precision wavemeter. (iii) The measurement at different beam energies, and with parallel and anti-parallel laser and ion beams, can be used to eliminate an offset voltage from the relations (7) and (3), if the main acceleration voltage is measured precisely.

This can be checked independently by the remeasurement of a well-known and sufficiently large atomic energy difference. (iv) With calibrated laser-frequency tuning for parallel and anti-parallel beams the constant beam energy essentially cancels out in the averaging of the measured frequency intervals[54]. For example, the isotope shift $\delta\nu^{AA'}$ between the two isotopes A and A' is given to first order by the expression

$$\delta\nu^{AA'} = \frac{1}{2}\{(\nu_+^{A'} + \nu_-^{A'}) - (\nu_+^{A} + \nu_-^{A})\} . \qquad (18)$$

A different combination of the measured frequencies

$$\frac{\nu_+^{A} - \nu_-^{A}}{\nu_+^{A'} - \nu_-^{A'}} = \frac{\sqrt{m_{A'}}}{\left(1 + \frac{\delta\nu^{AA'}}{\nu_o}\right)\sqrt{m_A}} \qquad (19)$$

gives the atomic mass of the isotope A' from the known mass of the isotope A. Although such a measurement can be rather precise (of the order 10^{-6}), the practical application to unstable isotopes may play a minor role, as there are new developments of rf mass spectrometers especially designed for this application[55,56].

For historical reasons, a few experiments were performed with beams intersecting at a small angle. This geometry avoids the optical pumping outside the observation region at the expense of resolution. The standard solution of this problem is the Doppler switching, i.e. the tuning into resonance within an insulated Faraday cage at non-zero potential. As this works only with ions, the fluorescence observation on neutralized beams should be close to the charge-exchange region. To some extent the excitation and optical pumping in front of the observation volume can be avoided by Zeeman-detuning of the participating energy levels[53], or exploited to achieve strong signals by the use of two lasers[57].

As the spectroscopy on ions often involves high-lying metastable states, the metastable population in the ion source is a crucial point. It is difficult to measure, and the estimates for various ion sources scatter between 10^{-6} and 10^{-2} [58-60]. A more quantitative systematic investigation of the best conditions for metastable beam production would certainly be useful. The situation is better under control for neutral atoms whose metastable states are populated by specific charge-transfer reactions. Here the population can easily reach a few tenths of the total beam intensity.

The commonly used fluorescence detection has to cope with a considerable background from scattered laser light. In fact, most experiments avoid to detect on the excitation wavelength and use the decay branch to a third state, selected by optical filters. If such a decay is weak or does not exist, the background has to be rejected by careful shaping of the laser beam profile and a suitable detection geometry which eliminates the scattered light with blackened diaphragms[11]. It has been shown in many experiments on weak beams of radioactive isotopes that a good photon-collection efficiency is compatible with a rather low background (see Section 5 and in particular[61]). The Doppler shift between laser light and fluorescence can be discriminated by a narrow-band interference filter[58], but this implies a very small angular acceptance of the detection system.

4.2 Laser-rf and Related Techniques

In classical atomic spectroscopy the hyperfine structures of ground or metastable states are measured with very high precision by rf techniques like atomic beam magnetic resonance (ABMR) which has no analogue in ion spectroscopy. Optical pumping-rf experiments have been performed only on a few alkali-like ions stored in a buffer gas[62] or an ion trap (cf. Part C, Chapter 5 by G. Werth). On the other hand, the laser interaction with a fast ion beam can be used to detect

rf resonances. The standard set-up (Fig. 5) corresponds to a Rabi type ABMR experiment in which the A magnet is replaced by an optical pumping zone and the B magnet by a fluorescence detector. Both the A and B zones can be tuned into optical resonance by an electrical potential on the Faraday cages. A coaxial rf transmission line gives a sufficiently uniform rf field with a transit time of a few μs. Experiments of this type were performed on the hyperfine structure of a few low-lying odd-parity states in U II[63] and the metastable 5d $^2D_{3/2}$ state in Ba II[64], while earlier approaches on 5d $^4D_{7/2}$ in Xe II[59] and 2 $^3S_1$ in Li II[65] used intersecting beams at small or right angles. In all cases the set-up is rather similar to the original proposal for an optical pumping rf technique by Kastler[3] and to the ABMR-LIRF technique on thermal atomic beams (cf. Part A, Chapter 10 by S. Penselin). The ultimate resolution limit with fast beams is given by the transit-time broadening of the order 100 kHz.

Of course, the possible combinations of laser-rf double resonance include all schemes that have been applied to thermal atomic beams. Thus for neutral atoms one can apply the laser and rf fields simultaneously as in conventional optical pumping experiments. This has been studied in the Na-D lines[66] where Zeeman transitions in the ground-state hyperfine structure were recorded. Due to the well-defined interaction time of the atoms with the rf field the line shape was in very good agreement with the Majorana formula. The monoenergetic beams even allow the observation of Zeeman structures in a static-field experiment[66,67]: The alignment of the Na I ground state or the Ba II metastable states by polarized laser light reduces the fluorescence intensity, and the free Larmor precession in a static magnetic field gives rise to a modulation of this fluorescence as a function of the field (Fig. 6). Both the rf transition frequency and the Larmor fringes essentially measure the g_F-factor $g_F = g_J/2I+1$ in the low-field limit, which may help to obtain unambigous nuclear spins (cf. Section 5).

However, this procedure can also be applied to diamagnetic atoms with $^1S_0$ ground states where the free nuclear precession is observed in fields of a few kG[68]. Such experiments are important for radioactive elements such as radium, where the magnetic moments in a long sequence of isotopes (cf. Section 5) can be calibrated by a direct g_I measurement of at least one isotope.

4.3 Nonlinear Spectroscopy

The inherent resolution of collinear-beam spectroscopy is still limited by the residual Doppler broadening. In beams with a broad velocity distribution the labeling of one velocity class by optical pumping, probed in a second Doppler-tuning zone, was exploited already before narrow Doppler widths were achieved[6,7,69,70]. The complete elimination of the first-order Doppler effect in resonant two-photon absorption on Ne I has been discussed in Section 3.3, in connection with a precision measurement of the relativistic Doppler effect. A similar experiment was performed on In I, where the 29p Rydberg state was excited from 5p $^2P_{3/2}$ via 6s $^2S_{1/2}$ and detected by field ionization[71]. The line width caused by the laser jitter can be reduced to the transit-time limit of a few 100 KHz.

Classical saturated absorption experiments on fast beams require different laser wavelengths to saturate and probe the same transition. However, a three-level system in V or Λ configuration can be realized to use the same direct and retro-reflected laser beam[72] interacting with the velocity class ß under the condition

$$ß = \frac{\nu_2 - \nu_1}{\nu_2 + \nu_1} , \qquad (20)$$

where ν_1 and ν_2 are the two atomic transition frequencies. This situation is shown in Fig. 7. Simultaneous resonance of the atoms on both transitions gives a reduction of population

of both the excited levels of the V configuration. The Λ configuration includes two metastable states, and the laser field burns holes into their velocity distribution which appear as peaks on the other side. At simultaneous resonance the strong coupling of all three states gives rise to increased emission. In both configurations the saturation signals are Doppler-free to first order, with a homogeneous line width given by $1/2(1/\tau + 2/T)$, where T is the transit time and τ is the excited-state lifetime. Experimental curves for the V case in Ne I 3s $[3/2]_2$ - (3p' $[3/2]_2$, $[3/2]_1$) are shown in Fig. 8 which demonstrates that the first-order Doppler effect is eliminated in the hole-burning dip, while the Doppler-broadened structure is shifted by post-acceleration. The Ne I experiment[72] yielded precision wave numbers of three transitions between the $2p^5$ 3s and $2p^5$ 3p' configurations of Ne I. Similarly, the Λ case was realized in the Ca I transitions ($4s4p\ ^3P_2$, $^3P_1$)-$4s5s\ ^3S_1$[72]. Another detailed study of this system with two copropagating laser fields and the involved coherent two-photon processes[73] gave a quantitative description of the observed dispersive and absorptive line shapes.

4.4 Transient Phenomena

The observation of transient effects is closely connected to the feature of Doppler switching by sudden changes of the ion velocity. Applications include cascade-free lifetime and quantum beat measurements by observation of the free decay after a short excitation region. Following the first experiments by Andrä[5] the alternative to produce a short excitation pulse by crossing the ion and laser beams has been applied extensively (cf. Part B, Chapter 20 by H.J. Andrä).

Silverans et al.[74] studied interference effects between ground (or metastable) and excited states in a set-up which is analogous to Ramsey's separated microwave field method. In comparison with other optical experiments, the interference conditions are easy to establish with fast ion beams, and the observed fringes are consistent with a Fourier analysis of the evolution in time of the laser frequency probed by the ions[75].

4.5 Spectroscopic Results

It is not surprising that most results in atomic spectroscopy were obtained on singly-charged ions which are difficult to prepare for the usual Doppler-free techniques on thermal samples. On the other hand, the fast-beam technique has certain advantages also on neutral atoms, such as the availability of metastable beams, the sensitivity and the Doppler-tuning.

Few-electron systems

Experiments of rather fundamental importance are those performed in the few-electron systems for which theory can provide accurate predictions of spectroscopic data. The first collinear-beam experiment on the simplest molecule HD^+ [12], and the possibility of a redetermination of the Rydberg constant on H atoms[26] point to this category of experiments. Also the two-electron atom He and the members of its isoelectronic sequence Li^+, Be^{++}, etc. have been treated theoretically by advanced perturbation methods, and the $2\,^3P$ fine structure of He is the source of one of the most accurate values of the fine structure constant α[76]. While the He I spectrum, and in particular the fine and hyperfine structures of the low-lying triplet states are known with high precision, the sprectroscopy on the He-like ions was handicapped by the poor resolution achieved under plasma conditions or with beam-foil excitation. Quantum beat measurements, which have a limited scope in the scale of atomic frequencies, yielded first precise hyperfine structures of the $1s2p\,^3P$ levels of Li II (cf. Chapter 20 by H.-J. Andrä). In a Doppler-tuned ion beam laser experiment Fan et al.[58,77] resolved the complete hyperfine structure of the triplet $2\,^3S_1 - 2\,^3P_J$ at 5485 Å for both stable isotopes ^6Li and ^7Li, using a beam of metastable Li^+ ions from a sputter source. The line width was 450 MHz, and an obvious improvement in the beam energy spread would make this experiment competitive with a more recent one[78] using saturation spectroscopy on a low-energy (200 eV) Li^+ beam. In contrast to earlier

measurements all three approaches confirm the many-body calculations[79] which were believed to be accurate within the present experimental errors of 10^{-4}.

An absolute wavelength measurement on the same transitions $2\,^3S_1 - 2\,^3P_J$ was performed by Holt et al.[60] to improve the experimental value of the differential Lamb shift (cf. Part A, Chapter 4 by A.M. Ermolaev). As in fast-beam experiments the absolute wave numbers depend critically on the knowledge of the Doppler shift,

$$\nu_o = \gamma(1 \pm \beta \cos\Theta)\,\nu_{1,2} \tag{21}$$

for a small intersection angle Θ which was chosen for technical reasons, β from the beam energy was largely eliminated by the use of two counter-propagating laser beams with the frequencies ν_1, ν_2. Stabilizing these frequencies on suitably chosen I_2 absorption lines required a small Doppler detuning $|\beta_1-\beta_2| \ll \beta$, but still the expression for the wave number

$$\nu_o = \frac{\gamma_1\gamma_2\,(\beta_1+\beta_2)}{(\gamma_2\beta_2/\nu_1) + (\gamma_1\beta_1/\nu_2)} \tag{22}$$

is quite insensitive to an unknown offset in the absolute beam energy. The results, after elimination of the hyperfine structure, are in good agreement with the theoretical values for both the fine structure[80] and the Lamb shift[81].

More recently, the extensive studies of the system $2\,^3S_1 - 2\,^3P_J$ in $^6Li^+$ and $^7Li^+$ by the Heidelberg group[65,78,82-84] have confirmed and improved all the earlier results from collinear laser spectroscopy - including the absolute wavelengths, the fine and hyperfine structures and the isotope shift. These experiments use the alternative technique of crossed-beam saturation spectroscopy combined with microwave resonance, taking advantage of the long interaction times in a low-energy Li^+ beam. Still, it seems that the considerable improvements are rather due to the skilful design of the experiments than to a principal advantage of the technique.

Transition energies and lifetimes

Only in exceptional cases precise atomic transition energy measurements can add relevant information to the tabulated energy levels[85,86]. Examples were given in connection with the few-electron system Li^{+} [60], and the Ne I spectrum[72] which has a considerable importance as a secondary wavelength standard and for the precision measurement of the relativistic Doppler shift[49]. In complex spectra the selective excitation may facilitate the classification of lines, in particular if combined with lifetime measurements. Thus a rather systematic study of U II transitions from the low-lying odd configurations f^3s^2, f^3ds and f^3d^2 has been demonstrated[87]. The excited-state lifetimes were measured by cw-laser modulation. The access to long-lived excited states by charge transfer collisions gives interesting possibilities to explore the poorly known parts of a level scheme. For highly-charged ions it has been pointed out[88] that the charge-transfer electron capture leads to Rydberg levels whose separation energies are in the optical spectral range.

Lifetime measurements with the conventional beam-foil replaced by laser excitation are discussed by H.-J. Andrä (Part B, Chapter 20).

A special wavelength measurement was recently performed in the second, 7s-8p resonance doublet of Fr I[89], of which the first optical lines, 7s-7p were discovered only a few years ago[90,91]. Here, the motivation for a collinear-beam experiment was the sensitivity to locate the narrow resonances within the estimated range of 100 Å, on a beam of 10^9 atoms/s for the isotope ^{212}Fr which has a half-life of 20 min. The francium ion beam was produced at ISOLDE from a thorium carbide target by spallation with 600 MeV protons, and neutralized by charge exchange with cesium. The optical spectroscopy on the heaviest alkali element provides a stringent test of the present theory of heavy atomic systems including strong relativistic contributions[92,93].

Hyperfine structure and isotope shift

Following the experimental tests on ions which have accessible transitions within the range of the first cw laser dye Rhodamin 6G, a series of experiments yielded results on the hyperfine structure and isotope shift of Xe^+ ($5p^4\ 5d\ ^4D_{7/2} - 5p^4\ 6p\ ^4P_{5/2}$) [14,59,94,95] and Ba^+ ($5d\ ^2D_{3/2,5/2} - 6p\ ^2P_{3/2}$) [96,97,52,98,64]. Of these, the alkali-like Ba II spectrum is of special interest for the theoretical or semi-empirical description of the atomic structure. The considerable field shift in the 5d-6p transitions [96,52] points to a large screening of the core s-shells by the 5d electron in agreement with theoretical calculations [99]. A precision measurement [98] even reveals a slight spin dependence of this effect within the doublet. Correspondingly, the 5d hyperfine structures in $^2D_{3/2}$ and $^2D_{5/2}$ are distorted by a non-vanishing contact term from core polarization. Precision measurements of these hyperfine structures by laser-rf spectroscopy [64,100], including a thorough investigation of possible light shifts [101], are sensitive to the second-order corrections due to a mutual perturbation of the fine structure levels. They indicate a non-vanishing hyperfine anomaly for the $^2D_{3/2}$ state. Many-body perturbation theory including correlation contributions reproduces rather well the experimental A-factors and can be used to determine independent values of the nuclear quadrupole moments from the B-factors. They agree well with the adopted semi-empirical values including the Sternheimer correction [61].

A more transparent situation is met in the resonance doublet 6s-6p of Ba II where the isotope shift is dominated by the direct contribution of 6s in the $^2S_{1/2}$ ground state. The experimental observation of different field shifts in the transitions to $^2P_{1/2}$ and $^2P_{3/2}$ [102] gives a direct access to the relativistic $p_{1/2}$ electron density at the nucleus which is in accordance with a semi-empirical estimate.

The motivation for hyperfine structure and isotope shift studies in the iso-electronic case of Ra II and in Ra I came originally from nuclear physics. After early measurements of the atomic energy levels on the long-lived ^{226}Ra[103], the isotope shifts and the hyperfine structures of the odd-A isotopes remained inaccessible until recently[104]. The extraction of nuclear moments required the analysis of the electronic hyperfine fields which was performed in on-line collinear-beam studies of several transitions involving the 7s $^2S_{1/2}$ and 7p $^2P_{1/2}$ states of Ra II and all states of the 7s7p configuration of Ra I[105]. The semi-empirical modified Breit-Wills theory[106] or equivalently the effective operator formalism[107] are shown to be valid also for the heaviest two-valence-electron atom with strong relativistic contributions to the wave function. The experiment initiated several ab-initio atomic structure calculations[108-111] which can be tested in additional experiments including the direct g_I-factor measurement (cf. Section 4.2) and the spectroscopy in the near-UV Ra II resonance line to 7p $^2P_{3/2}$.

Various other hfs investigations have been carried out on ions which have a complex electronic structure. They are usually treated within the effective operator formalism[107] whose parameters are related to radial integrals $\langle r^{-3} \rangle$ (see e.g. Part A, Chapter 10 by S. Penselin) for which theoretical or semi-empirical values are introduced to determine in particular the nuclear quadrupole moments. Thus for Eu II the hfs of the multiplet $4f^7(^8S)5d\,^9D$, measured in transitions to $4f^7 6p$[112], yield another independent value of the first discovered nuclear quadrupole moment[113]. Similarly, the analysis of the hfs of the $5f^3 7s^2$, $5f^3 6d7s$ and $5f^3 6d^2$ configurations from the laser-rf experiment on U II[63] gives the 7s contact interaction term and a new value for the magnetic moment of ^{235}U. All metastable $5d^2$ and 5d6s levels of La II were studied in a number of transitions[114] and the extracted hfs parameters including two-body far-configuration mixing were compared with ab-initio evaluations[115]. The analysis also gives a corrected value of the quadrupole moment of ^{139}La. In one

of the transitions ($5d^2\ ^3F_4$ - $5d4f\ ^3F_4$) a new type of $\Delta F = \pm 2$ transitions was observed and ascribed to a three-quantum dipole process[116]. In the rare-gas spectrum of Cs II the hfs of $6p\ [3/2]_2$, excited from the metastable $5d\ [3/2]_2$ level[117], was compared with a semi-empirical evaluation. A similar measurement and analysis had been performed using the in-flight hole-burning technique of Gaillard on the $5s\ [3/2]_2$ - $5p[1/2]_1$ transition of Rb II[70]. Transitions from $3d^2$ to 3d4p in Sc II were examined within the scope of stellar abundance analysis[118]. The measured hfs show that theoretical predictions involve considerable uncertainties for the interpretation of line shapes in the spectra from celestial objects.

The isotope shifts of light elements give absolute values of the specific mass effect caused by electron momentum correlations. Studies of transitions of the type $3p^{n-1}3d$ - $3p^{n-1}4p$ in Ar II (n = 5), Cl II (n = 4) and S II (n = 3)[119,120] indicate a strong correlation of the 3d electron with the inner p-shells which is much larger than in the neutral spectra. (The same transitions in Ar II were also used to study optical pumping and the Hanle effect which yielded the lifetimes of the 4p levels[121]). The experimental mass shifts are somewhat overestimated by calculations based on Hartree-Fock wavefunctions, although the trends are very well reproduced. Generally, it seems that only refined theoretical methods may give quantitative predictions of the mass shift which in the intermediate mass range limits the accuracy of changes in the mean square nuclear charge radius extracted from the isotope shifts (cf. Section 5.1).

5. Spectroscopy on Unstable Isotopes

It may be surprising to find the most extensive application of collinear laser fast-beam spectroscopy in a field[122] which a priori has little connection with the special features of this technique. Neither the Doppler shift nor the accessibility of ionic states play a decisive role for the on-line experiments on radioactive isotopes from nuclear reactions. However, most of the problems encountered in the preparation of a sample of free atoms (cf. Part B, Chapter 17 by H.-J. Kluge) are solved by a combination of the fast-beam technique with the well-established concept of on-line isotope separation. The isotope separators (with ISOLDE at CERN[123] as an outstanding example) provide the unstable species in the form of ion beams whose phase-space volume is well matched to the requirements of collinear spectroscopy.

Obvious advantages allow the investigation of nearly any element which is available from the isotope separator:

(i) Convenient optical transitions - including those from metastable states - can be chosen from the spectra of the neutral atom or the singly-charged ion.

(ii) The sensitivity, owing to efficient excitation within the narrow Doppler profile, is essential for the weakly produced isotopes far from stability.

(iii) The Doppler effect provides a large tuning range and easy control of the effective wavelength of the laser light.

(iv) Fluorescence detection gives greatest versatility and specialized particle detection schemes may further improve the sensitivity.

(v) High resolution yields sufficiently accurate hyperfine structure parameters and isotope shifts.

5.1 Hyperfine Structure and Isotope Shifts

We shall briefly review the relationship between spectroscopic observables and nuclear properties[124,125,126]. These properties include spins, magnetic dipole and electric quadrupole moments, as well as the variation in the mean square charge radius within a sequence of isotopes. They manifest themselves in the hyperfine structures and isotope shifts. The hyperfine energies of the different F states within a hyperfine multiplet $|J - I| \leq F \leq J + I$, given by the well-known formula

$$W_F = \frac{1}{2} KA + \frac{(3/4)\ K\ (K+1) - I\ (I+1)\ J\ (J+1)}{2\ I\ (2I-1)\ J\ (2J-1)}\ B \qquad (23)$$

with $K = F\ (F+1) - I\ (I+1) - J\ (J+1)$, are determined by the nuclear spin I, the magnetic dipole interaction constant

$$A = \mu_I\ H_e(0)/IJ \qquad (24)$$

and the electric quadrupole interaction constant

$$B = eQ_s\ \varphi_{JJ}(0). \qquad (25)$$

The nuclear moments μ_I and Q_s can be extracted from A and B using empirical or theoretical values for the magnetic hyperfine field $H_e(0)$ and the electric field gradient $\varphi_{JJ}(0)$ at the nucleus. Apart from hyperfine anomaly corrections $H_e(0)$ is usually known from direct g_I-factor measurements ($g_I = \mu_I/I\mu_N$) on the stable isotopes. $\varphi_{JJ}(0)$ is taken from semiempirical or theoretical analyses, unless precise values are available from the hfs of muonic atoms.

Similarly, the isotope shift $\delta\nu^{AA'}$ of an optical transition is related to the change in the nuclear mean square charge radius $\delta\langle r^2\rangle^{AA'}$ between the isotopes A and A' by

$$\delta\nu^{AA'} = F\delta\langle r^2\rangle^{AA'} + M\ \frac{A' - A}{A'A} \qquad (26)$$

where the electronic factor F of the field shift term is proportional to the change of the electron charge density at the nucleus in the optical transition. The second term represents the mass shift due to the change of nuclear recoil energy. In simple (s-p or s^2-sp) transitions of heavy elements, where F is large and (A'-A)/A'A is small, one can usually neglect the specific mass effect of electron momentum correlation and assume $M = \nu/1836(1\pm1)$ for the transition frequency ν[126]. Isotope shifts in other transitions can be related to those by the King plot procedure. Another advantage of the s-p transitions consists in the reliability of semi-empirical or theoretical values of F which are mainly determined by the s-electron density. Shielding, relativistic and finite nuclear size effects and the contribution of higher-order moments of the nuclear charge distribution are accounted for by corrections. These and the complications from configuration mixing are discussed in more detail by K. Heilig and A. Steudel in Part A, Chapter 7.

5.2 Review of Experiments

The virtues of collinear-beam spectroscopy for nuclear systematics are best demonstrated by the chart of nuclides (Fig. 9) on which the investigated longer chains of unstable isotopes are marked by solid frames. The majority of the results was obtained from collinear-beam measurements, while the rest is shared by a number of more specialized techniques (see e.g. refs. (126-128)). In a few cases the measurements cover nearly all known isotopes, and examples of nuclear physics results will be given in Section 5.4.

The individual experiments are compiled in Table 1 which is arranged in the order of elements and gives the isotopes and transitions that were investigated. A separate column shows the production reactions and the accelerator or reactor facility used for the on-line work. As the most extensive experimental programme is concentrated at ISOLDE, the standard set-up for these measurements will be outlined in the following.

5.3 Experimental Set-up and Procedure

Fig. 10 shows the essential parts of the ISOLDE apparatus[61]. Indicated are the target-ion source assembly and the mass-separator magnet from which the ion beam is guided to the particular experimental set-up. For collinear laser spectroscopy the 60 kV acceleration voltage is stabilized[154] to fluctuations and long-term drifts of less than 10^{-5}. This is particularly important because of the high pulsed current load (10 mA) due to ionization of the target area by the 2 μA proton beam of 600 MeV.

Inside the apparatus the ion beam is deflected into the laser beam axis and neutralized in a charge-exchange cell at a variable potential of ± 10 kV. This gives a Doppler-tuning range for the fast atoms of typically 80 GHz. The fluorescence photons are collected along 20 cm by cylindrical optics and a light pipe. For spectroscopy on ions the potential is applied to the electrically insulated observation chamber instead of the charge-exchange cell.

The measurement consists in a comparison of the resonance positions of different isotopes. The result of such a measurement[143,145] is shown in Fig. 11 for the example of Dy I (4212 Å). The hfs of the odd-A isotope, ^{151}Dy, and the single components of the stable doubly-even isotopes, ^{156}Dy and ^{158}Dy, are displayed versus the total acceleration voltage U which is the sum of the constant isotope separator voltage and the Doppler-tuning potential. To first order the change ΔU in U is related to the change Δm in the atomic mass m and the isotope shift $\Delta\nu^{AA'}$ for a transition with frequency ν_o by

$$\frac{\Delta U}{U} = \frac{\Delta m}{m} - \frac{\Delta\nu^{AA'}}{\nu_o}\left(\frac{2mc^2}{eU}\right)^{1/2} . \qquad (27)$$

This indicates that the same relative precision (of e.g. 10^{-4}) of both the small ΔU and the large U is adequate for the measurement of $\Delta\nu$, and only the stability of U has to correspond to the initial energy spread of the ions to avoid broadening. The cyclic

measurement on a sequence of isotopes and fast scanning help to reduce further the errors introduced by fluctuations or drifts of the voltages, the laser frequency or the beam intensities.

The sensitivity achieved in favourable transitions is illustrated in Fig. 12 for the example of the $7s^2\ ^1S_0$ - $7s7p\ ^1P_1$ resonance line of Ra I (4826 Å). The weakest beam of an even radium isotope, used in this experiment[104,153], was about 10^4 atoms/s. Odd isotopes require 10 to 100 times stronger beams, depending on their hyperfine structure. For ^{208}Ra, the recording of a resonance with a signal-to-noise ratio of 10 in 50 channels took 10^3s, which means that about 10^7 atoms, or 4 fg of radium, have passed through the apparatus during the measurement. The signal was 200 counts/s, arising from about 10 excitations per atom and a total photon-detection efficiency of 0.2 %. This has to be compared to a background of 10^4 counts/s of which the dominant part is due to stray light. In general, the sensitivity is reduced by smaller transition probabilities, hyperfine structure splittings and optical pumping. Depending on these conditions, the practical limits lie between 10^4 and 10^7 atoms/s.

5.4 Results in Nuclear Physics

To show the impact of laser spectroscopy on nuclear physics we discuss selected results from the aspect of information about the nuclear structure. Owing to collinear-beam spectroscopy it has now been possible to study a number of interesting regions all over the chart of nuclides.

Spins

The direct measurement of nuclear ground (and isomeric) state spins from the hfs is of basic importance for all indirect spin assignments of nuclear spectroscopy. The spins provide a stringent test of theoretically predicted single-nucleon

states which are obtained by spherical or deformed shell-model calculations. Very often the spins have given first evidence of unexpected phenomena. A recent example is the spin sequence of the heavy odd-A radium isotopes $^{221-229}Ra$ [104] which fits perfectly into the picture of parity-mixed neutron orbitals in a reflection asymmetric nuclear potential [155]. In other words, nuclei may have intrinsic octupole-deformed shapes, although static electric octupole moments are forbidden by parity conservation.

Magnetic Moments

The magnetic dipole moments are sensitive to details of the single-nucleon wavefunctions. Thus the mixture of opposite-parity orbitals in the octupole-deformed potential gives small magnetic moments in between the two Schmidt lines for $j = l_1 + 1/2$ and $j = l_2 - 1/2$ nucleons. Quantitative calculations [155,156] reproduce rather well the experimentally observed moments [104,105] of $^{221-229}Ra$. In such calculations the single particle is coupled to a rotor core and the numerous modes of core polarization are usually subsumed under an effective gyromagnetic factor $g_s' \approx 0.6 - 0.7\ g_s(\text{free})$ where the latter refers to the free nucleon.

A quantitative theoretical understanding of the magnetic moments is established only for nuclei which have one particle or hole in a doubly-magic core. For these nuclei an effective operator for the moment can be written as [157]

$$\mu_{eff} = (g_s + \delta g_s)\ s + (g_l + \delta g_l)\ l + g_p\ [s \times Y^2]^{(1)}. \qquad (28)$$

The spin and orbital gyromagnetic ratios g_s and g_l are the free nucleon values; δg_s and δg_l are caused by both core polarization and meson exchange. The last term, arising from the dipole-dipole interaction, is a rank one tensor product of spherical harmonic of order two, Y^2, and the spin operator. The separate contributions of δg_s, δg_l and g_p can be extracted

from experimental data including high-spin and low-spin states and also calculated by theory. For the rather extensive evaluation of the neighbourhood of ^{208}Pb[157] the only gap in the systematics has been closed recently by the hfs measurement on ^{207}Tl[148] which is the only known heavy nucleus with a single $s_{1/2}$ particle or hole. In this case both the g_l and g_p terms vanish, and the isolated δg_s accounts for mainly core polarization effects which reduce the magnetic moment from the free-proton value of 2.79 μ_N to 1.88 μ_N within a few percent of the best theoretical predictions.

Since ^{146}Gd (Z = 64, N = 82) behaves very much like a doubly-magic nucleus[158], the neighbouring ^{145}Eu (Z = 63) is of similar nature as the nuclei around ^{208}Pb, and to either side the long sequence of $d_{5/2}$ proton states in the odd-A isotopes $^{141-151}Eu$ show a gradual quenching of the single-particle moments due to the admixture of collective states (Fig. 13). The onset of strong deformation between the two stable isotopes ^{151}Eu and ^{153}Eu gives a drop in the magnetic moment, because the $d_{5/2}$ shell model state becomes a nearly pure [413 5/2] Nilsson state with a deformation of $\beta_2 \approx 0.30$. This goes along with the sudden increase of the nuclear quadrupole moment which was discovered 50 years ago in the famous work of Schüler and Schmidt[113]. Fig. 13 combines the results of two collinear-beam experiments performed at ISOLDE[141] and at the Gatchina isotope separator[139].

Quadrupole Moments

Most spectroscopic quadrupole moments are considerably larger than the single-particle values of the spherical shell model. This is true even for nuclei near double shell closures. For example, $Q(^{145}Eu) = 0.29$ b exceeds the roughly estimated single-particle value $Q_{sp} = 0.13$ b by more than a factor of 2. Collective effects described by dynamic or static deformation become dominant as one goes away from magic proton or neutron numbers. However, the spectroscopic quadrupole moment Q_s is

not directly related to the intrinsic quadrupole moment Q_o which describes the nuclear shape in terms of a deformation parameter β_2,

$$Q_o = \frac{3}{\sqrt{5\pi}} ZR^2\beta_2 \ , \qquad (29)$$

where R is the nuclear radius. Only in the limit of large deformation the strong coupling between the spin of the odd particle and the nuclear deformation axis gives the simple projection

$$Q_s = \frac{I\ (2I-1)}{(I+1)\ (2I+3)}\ Q_o \ . \qquad (30)$$

In the transitional regions one finds the situation that Q_s changes systematically and reverses the sign under sequential filling of a neutron shell. This is described by a change from the decoupled to the strongly coupled scheme, going along with a change of the projection Q_s/Q_o from negative to positive values for the same nuclear spin. In such a sequence the intrinsic quadrupole moment Q_o may be almost constant. This phenomenon was first observed in the $i_{13/2}$ isomers of $^{185-199}$Hg[159] and explained quantitatively by Ragnarsson[160]. Similar cases are pointed out by Ekström[161], and another example is given in Fig. 14 for the $f_{7/2}$ states of the rare-earth nuclides above the shell closure N = 82[144] which have been the subject of systematic measurements by collinear laser spectroscopy. Thus the quadrupole moments can be understood as an interplay between the collective and single-particle structure of the nucleus.

Mean Square Charge Radii and Nuclear Shape

According to eq. (26) the isotope shifts yield the changes of the mean square nuclear charge radii within the sequence of isotopes. These are largely insensitive to the single-particle structure and mainly reflect the collective properties of the nuclei. Even as a rough overall description of the radii

the liquid drop formula $R = R_o A^{1/3}$, with $R_o = 1{:}2$ fm, and $\langle r^2 \rangle = 3/5\ R^2$ is oversimplified, because protons and neutrons act differently on the charge radius. This is taken into account by the phenomenological droplet model[162,163] which allows for nuclear compressibility and neutron-skin effects: For nuclei of constant shape the variation $\delta\langle r^2 \rangle$ with the neutron number is nearly half the value given by the $A^{1/3}$ law. Deviations from this global behaviour arise from the shell structure and can be largely ascribed to deformation effects: The mean square radius of a spheroid which has the same volume as a sphere with $\langle r^2 \rangle_o$, is given by

$$\langle r^2 \rangle = \langle r^2 \rangle_o \left(1 + \frac{5}{4\pi} \langle \beta_2^2 \rangle\right). \qquad (31)$$

$\langle \beta_2^2 \rangle$ represents an average deformation parameter arising from either zero-point vibrations, or static deformation with $\langle \beta_2^2 \rangle = \beta_2^2$. This simple picture describes rather coherently most of the presently known $\delta\langle r^2 \rangle$ curves within long sequences of isotopes by

$$\delta\langle r^2 \rangle = \delta\langle r^2 \rangle_o + \frac{5}{4\pi} \langle r^2 \rangle_o\ \delta\langle \beta_2^2 \rangle\ . \qquad (32)$$

An example is given in Fig. 15, again for the case of europium[141]. Assuming $\beta_2 = 0$, i.e. spherical shape for ^{145}Eu next to the doubly-magic ^{146}Gd, one obtains $\beta_2 = 0.32$ for the strongly-deformed ^{153}Eu by the decomposition of $\delta\langle r^2 \rangle^{145,153}$ into the droplet and deformation contributions. This is in perfect agreement with deformation values from reduced transition probabilities B(E2) and from the spectroscopic quadrupole moment using eqs. (29,30). The detailed calculations include small corrections and higher-order terms in eqs. (29,32) which have been omitted for the sake of clarity.

Europium, which has been studied also in the first on-line experiments using multistep photo-ionization from a thermal atomic beam[164,165], continues a larger series of rare-earth elements investigated systematically at ISOLDE[143-145]. The main subject of these studies was the development of strong

deformation around N = 90 which occurs suddenly, i.e. between N = 88 and 90 in Nd (Z = 60), Sm (Z = 62) and Gd (Z = 64) which - like Eu - have stable isotopes in this region. On the other hand, the neutron-rich Ba (Z = 56) isotopes[61] and the neutron-deficient Yb (Z = 70) isotopes[27] behave smoothly. Including the measurements on Dy (Z = 66) and Er (Z = 68) Fig. 16[143-145] shows a clear Z-dependence in the onset of strong deformation which is represented by the peak value of the differential $\delta\langle r^2\rangle^{N-2,N}$ (Brix-Kopfermann diagram). The "jump" into deformation, known from the early work of Brix and Kopfermann[166,167] seems to be the exception which is related to the neighbourhoud of the semi-magic proton number Z = 64, stabilizing the spherical shape for the neutron numbers $N \leq 88$. It is important noting that this first systematic study on the unstable isotopes of a sequence of different elements has become possible by the flexibility of the collinear beam technique.

The simplification in the two-parameter description of eq. (32) becomes apparent with the prediction of a sizeable octupole deformation for the neutron-rich radium isotopes. In fact, the experimental $\delta\langle r^2\rangle$ values between the nearly-spherical ^{214}Ra (N = 126) and the heavier isotopes $^{220-232}$Ra[152,153] suggest a considerable higher-order deformation contribution. This can be taken care of by the addition of terms $\frac{5}{4\pi}\langle r^2\rangle_o$ $(\delta\langle\beta_3^2\rangle + \delta\langle\beta_4^2\rangle)$ to the expression of eq. (32), but the isotope shift can not distinguish between the different modes of deformation. It seems, however, that the inversion of the odd-even staggering, observed for ^{221,223,225}Ra[152,153] (Fig. 17), and also for the neighbouring ^{220,222}Fr[168] and ^{219,221}Rn[150,151] can be understood qualitatively as an effect of octupole correlations which are particularly pronounced in the odd-neutron isotopes[169]. A conclusive interpretation of this effect implies the quantitative understanding of the generally observed normal odd-even staggering. One can expect that the key information for this will be provided by the wealth of new data in rather different regions of the chart of nuclides.

A by-product of the isotope shift measurements on long isotopic chains and in different transitions is the possibility to draw King plots[126] of unprecedented accuracy. These provide an extremely sensitive test of the validity of eq. (26) which implies that the isotope shifts in different transitions, multiplied by the inverse mass shift factor $AA'/(A'-A)$, or more precisely $m_A m_{A'}/(m_{A'}-m_A)$, depend linearly on each other. This procedure also allows to relate the electronic factors F_i and the mass shift constants M_i of different transitions. A beautiful example of such a King plot is shown in Fig. 18 for the 4683 Å line ($7s\ ^2S_{1/2}$ - $7p\ ^2P_{1/2}$) in Ra II and the 4826 Å line ($7s^2\ ^1S_0$ - $7s7p\ ^1P_1$) in Ra I[105]. The accuracy is not only due to the inclusion of 17 isotopes between A = 208 and 230, but also to the considerably different isotope shifts on both sides of the magic neutron number N = 126 and the odd-even staggering.

5.5 Higher Sensitivity by Ionization

In all the described experiments the sensitivity limit of 10^4 - 10^7 atoms/s (cf. Section 5.3) arises from the low optical detection efficiency and the background due to stray light. Therefore, non-optical detection schemes are considered most promising for experiments on the isotopes with very low production rates. The stepwise laser resonance ionization with subsequent ion counting is well developed for pulsed lasers with high power, but low duty cycle, acting on samples of thermal atoms[170,171]. With fast beams this technique gives improved isotopic selectivity, due to the large Doppler shift and narrowing[172], but considerable duty cycle losses in sensitivity. These may be minimized by the high repetition rate of copper-vapour pumped dye lasers. Single-mode cw lasers are limited in power, and attempts are being made to achieve efficient ionization by the excitation to low Rydberg states[173,71]. They have to cope with optical pumping losses and resolved hyperfine splittings in the intermediate states.

A straightforward alternative is found in the state-selective collisional ionization of metastable atoms. By laser excitation they can be pumped to the ground state, which leads to a reduction of the ionization rate. Similar techniques were used in the early collinear-beam experiments on HD^+ by Wing et al.[12] and on Ba^+ by Gaillard et al.[69] who observed small changes in the ion beam current, due to slightly different neutralization or double-ionization cross-sections for the states involved in the optical excitation and decay. On the other hand, there are examples of strongly state-selective processes, such as the near-resonant charge transfer neutralization. Thus, Silverans has shown recently[174] that the excitation of Sr^+ in the 5s-5p resonance lines, followed by the decay to the metastable 4d levels, strongly affects the beam composition of ions and neutral atoms after passage through sodium or caesium vapour.

The collisional ionization scheme[175,176] is especially suitable for the rare gases whose first excited states lie about 10 eV above the $np^6\ ^1S_0$ ground states: The metastable J = 2 states of the configuration np^5 (n+1)s --designated (n+1)s $[3/2]_2$ -- about - 4eV from the ionization threshold are efficiently populated in charge exchange with caesium[24]. They are connected to the states of the configuration $np^5(n+1)p$ by strong transitions on the red. In a test experiment on krypton[175,176] the neutralized beam, superimposed with the laser beam, passed a differentially pumped gas cell after which the re-ionized part was deflected into a Faraday cup or an ion counter. The laser excitation from the 5s $[3/2]_2$ metastable to the 5p $[3/2]_2$ state at 7602 Å was followed by the decay cascade via 5s $[3/2]_1$ to the ground state (Fig. 19). Since the cross-section for electron stripping from the ground state (-14 eV) is much smaller than from the metastable state (-4 eV), this pumping leads to a reduction of the ion signal which can thus be used to detect the optical resonance.

Among various stripping gases, SO_2 gave the highest re-ionization efficiencies of 10 - 20 %, mainly limited by secondary processes, such as charge-transfer neutralization. At resonance, the flop-out signal in the ion current was about 40 %. In Fig. 19 a direct comparison with the simultaneously recorded fluorescence signal shows a gain in detection efficiency of more than a factor of 10^3. In principle, this ion signal is free of background. However, for the planned experiments on weak radioactive isotopes it will be essential to have low contamination of the beams with molecular ions or strong neighbouring masses from the isotope separator. In favourable cases, the radioactive decay may serve for detection, thus removing the possible background from stable beams.

5.6 Implantation of Polarized Atoms

The classical RADOP experiments are described by H.-J. Kluge in Chapter 17. Their sensitivity is based on the detection of the asymmetry in the radioactive ß-decay which provides an inherent spin detector for polarized nuclei. A combination of fast-beam spectroscopy with the RADOP scheme can be realized by optical pumping with circularly polarized light and subsequent implantation of the atoms into a suitable crystal lattice where the nuclear polarization is detected in their decay[177]. For short-lived isotopes this can offer interesting advantages including the sensitive detection of optical resonance, direct g_I-factor measurements by nmr on the implanted nuclei, and solid-state relaxation and hyperfine field studies. This technique was developed by the use of neutron-rich Rb isotopes from fission[178] and applied recently to determine the spin and magnetic moment of ^{11}Li[179]. About 10^3 atoms/s of this exotic nuclide are produced at ISOLDE from fragmentation of ^{181}Ta or ^{238}U. They were polarized by optical pumping in the resonance lines $2s\ ^2S_{1/2} - 2p\ ^2P_{1/2,3/2}$ (6707 Å) and implanted into a gold foil placed in a static magnetic field of about 1 kG. The optical resonances were detected by asymmetries of a few percent and yielded the ground-state hyperfine splitting. The result indicates a magnetic moment close to the Schmidt value of the $p_{3/2}$ shell-model proton state. It seems to be incompatible with theoretical predictions of a strongly deformed nuclear system of spin I = 1/2 and favours the shell-model description of a $p_{3/2}$ proton plus a doubly-magic (Z = 2, N = 8) core. More detailed information is expected from nmr experiments yielding the g_I-factor and the spectroscopic quadrupole moment. Due to its short half-live of 8.7 ms and long relaxation time, ^{11}Li is an ideal candidate for this technique, and for solid-state studies the much stronger produced isotopes ^{8}Li ($T_{1/2}$ = 842 ms) and ^{9}Li ($T_{1/2}$ = 178 ms) can be used as convenient probes.

6. Conclusion

It has been shown by means of examples that the collinear laser fast-beam technique has introduced many interesting aspects into the classical field of atomic spectroscopy. This discussion has not touched upon the promising applications to molecular ions including spectroscopy and reaction studies, as the physics involved is beyond the scope of this contribution. To date, it appears that a systematic application in atomic spectroscopy has been established in the work on radioactive nuclides, due to the sensitivity and resolution, but even more the ideal adaption of the spectroscopic method to the conditions of production.

The progress in the development of tunable and narrow-band UV lasers will give a new impact on ion spectroscopy, and future experiments may extend high-resolution spectroscopy to multiply-charged ions. In this context the laser cooling and spectroscopy of ions in a storage ring[180,181] is a particularly attractive possibility, although it will need a lot of ingenuity to solve both the physical and the technical problems.

References

1. H. Schüler, Z. Phys. 59, 149 (1930).
2. I.I. Rabi, S. Millman, P. Kusch, and J.R. Zacharias, Phys. Rev. 55, 526 (1939).
3. A. Kastler, J. Phys. Radium 11, 255 (1950).
   J. Brossel, A. Kastler, and J. Winter, J. Phys. Radium 13, 668 (1952).
4. J. Brossel and A. Kastler, C.R. Acad. Sci. (Paris) 229, 1213 (1949).
   J. Brossel and F. Bitter, Phys. Rev. 86, 308 (1952).
5. H.J. Andrä, A. Gaupp, and W. Wittmann, Phys. Rev. Lett. 31, 501 (1973).
6. M. Dufay, M. Carré, M.L. Gaillard, G. Meunier, H. Winter, and A. Zgainski, Phys. Rev. Lett. 37, 1678 (1976).
7. H. Winter and M.L. Gaillard, J. Phys. B 10, 2739 (1977).
8. H.J. Andrä, in Beam-Foil Spectroscopy, Vol. 2, Eds. I.A. Sellin and D.J. Pegg, Plenum Press, New York (1976), p. 835.
9. S.L. Kaufman, R. Neugart, and E.W. Otten, unpublished report, DFG Colloquium on Laser Spectroscopy, Bad Nauheim (May 1975).
10. S.L. Kaufman, Opt. Commun. 17, 309 (1976).
11. K.-R. Anton, S.L. Kaufman, W. Klempt, G. Moruzzi, R. Neugart, E.W. Otten, and B. Schinzler, Phys. Rev. Lett. 40, 642 (1978).
12. W.H. Wing, G.A. Ruff, W.E. Lamb, jr., and J.J. Spezeski, Phys. Rev. Lett. 36, 1488 (1976).
13. Th. Meier, H. Hühnermann, and H. Wagner, Opt. Commun. 20, 397 (1977).
14. R.A. Holt, S.D. Rosner, and T.D. Gaily, Phys. Rev. A 15, 2293 (1977).
15. W.H. Wing, in Laser Spectroscopy III, Eds. J.L. Hall and J.L. Carlsten, Springer, Berlin (1977), p. 69.
16. J.T. Moseley, P.C. Cosby, J. Durup, and J.B. Ozenne, J. Physique (Paris) 40, C1-46 (1979).

17. A. Carrington and P.J. Sarre, J. Physique (Paris) 40, C1-54 (1979).
18. M. Horani, H.H. Bukow, M. Carré, M. Druetta, and M.L. Gaillard, J. Physique (Paris) 40, C1-57 (1979).
19. A. Carrington, Ann. Isr. Phys. Soc. (Israel) 4, 231 (1980).
20. M.L. Gaillard, in Atomic Physics 8, Eds. I. Lindgren, A. Rosén, and S. Svanberg, Plenum Press, New York (1982), p. 467.
21. A. Carrington and T.P. Softley, in Molecular Ions: Spectroscopy, Structure and Chemistry, Eds. T.A. Miller and V.E. Bondybey, North-Holland, Amsterdam (1983), p. 49.
22. H.S.W. Massey and H.B. Gilbody, Electronic and Ionic Impact Phenomena, Vol. 4, Clarendon, Oxford (1974).
23. D. Rapp and W.E. Francis, J. Chem. Phys. 37, 2631 (1962).
24. G.E. Ice and R.E. Olson, Phys. Rev. A11, 111 (1975).
25. F.W. Meyer, C.J. Anderson, and L.W. Anderson, Phys. Rev. A15, 455 (1977).
26. E. Arnold, T. Kühl, E.W. Otten, and L. von Reisky, Phys. Lett. 90A, 399 (1982).
27. F. Buchinger, A.C. Mueller, B. Schinzler, K. Wendt, C. Ekström, W. Klempt, and R. Neugart, Nucl. Inst. Meth. 202, 159 (1982).
28. M. Bacal, A. Truc, H.J. Doucet, H. Lamain, and M. Chrétien, Nucl. Inst. Meth. 114, 407 (1974).
29. M. Bacal and W. Reichelt, Rev. Sci. Instr. 45, 769 (1974).
30. J.C. Brenot, J. Pommier, D. Dhuicq, and M. Barat, J. Phys. B 8, 448 (1975).
31. P.M. Koch, Opt. Commun. 20, 115 (1977).
32. B. Schinzler, Thesis, Mainz (1980).
33. C. Reynaud, J. Pommier, Vu Ngoc Tuan, and M. Barat, Phys. Rev. Lett. 43, 579 (1979).
34. C.-J. Lorenzen, K. Niemax, and L.R. Pendrill, Opt. Commun. 39, 370 (1981).
35. J. Kowalski, R. Neumann, S. Noehte, R. Schwarzwald, H. Suhr, and G. zu Putlitz, Opt. Commun. 53, 141 (1985).

36. E.W. Otten, private communication.

37. J.E.M. Goldsmith, E.W. Weber, and T.W. Hänsch, Phys. Rev. Lett. 41, 1525 (1978).

38. S.R. Amin, C.D. Caldwell, and W. Lichten, Phys. Rev. Lett. 47, 1234 (1981).

39. O. Poulsen, Nucl. Instr. Meth. 202, 503 (1982).

40. H.E. Ives and G.R. Stilwell, J. Opt. Soc. Am. 28, 215 (1938); 31, 369 (1941).

41. H.I. Mandelberg and L. Witten, J. Opt. Soc. Am. 52, 529 (1962).

42. D.C. Champeney, G.R. Isaak, and A.M. Khan, Proc. Phys. Soc. 85, 583 (1965).

43. J. Bailey, K. Borer, F. Combley, H. Drumm, F. Krienen, F. Lange, E. Picasso, W. von Rüden, F.J.M. Farley, J.H. Field, W. Flegel, and P.M. Hattersley, Nature (London) 268, 301 (1977).

44. P. Juncar and J. Pinard, Rev. Sci. Instr. 53, 939 (1982).

45. P. Juncar, C.R. Bingham, J.A. Bounds, D.J. Pegg, H.K. Carter, R.L. Mlekodaj, and J.D. Cole, Phys. Rev. Lett. 54, 11 (1985).

46. J.J. Snyder and J.L. Hall, in Laser Spectroscopy, Eds. S. Haroche, J.C. Pebay-Peyroula, T.W. Hänsch, and S.E. Harris, Springer, Berlin (1977), p. 6.

47. O. Poulsen and N.I. Winstrup, Phys. Rev. Lett. 47, 1522 (1981).

48. M. Kaivola, N. Bjerre, O. Poulsen, and J. Javanainen, Opt. Commun. 49, 418 (1984).

49. M. Kaivola, O. Poulsen, E. Riis, and S.A. Lee, Phys. Rev. Lett. 54, 255 (1985).

50. B. Schinzler, W. Klempt, S.L. Kaufman, H. Lochmann, G. Moruzzi, R. Neugart, E.W. Otten, J. Bonn, L. von Reisky, K.P.C. Spath, J. Steinacher, and D. Weskott, Phys. Lett. 79B, 209 (1978).

51. W. Klempt, J. Bonn, and R. Neugart, Phys. Lett. 82B, 47 (1979).

52. R.E. Silverans, G. Borghs, G. Dumont, and J.M. Van den Cruyce, Z. Phys. A 295, 311 (1980).

53. G. Ulm, J. Eberz, G. Huber, H. Lochmann, R. Menges, R. Kirchner, O. Klepper, T. Kühl, P.O. Larsson, D. Marx, D. Murnick, and D. Schardt, Z. Phys. A 321, 395 (1985).

54. G. Borghs, P. De Bisshop, J.M. Van den Cruyce, M. Van Hove, and R.E. Silverans, Opt. Commun. 38, 101 (1981).

55. H. Schnatz, G. Bollen, P. Dabkiewicz, P. Egelhof, F. Kern, H. Kalinowsky, L. Schweikhard, H. Stolzenberg, and H.-J. Kluge, Nucl. Instr. Meth. A251, 17 (1986)

56. A. Coc, R. Fergeau, C. Thibault, G. Audi, M. Epherre, P. Guimbal, M. de Saint-Simon, F. Touchard, E. Haebel, H. Herr, R. Klapisch, G. Lebée, G. Petrucci, and G. Stefanini, Proc. 7th Int. Conf. on Atomic Masses and Fundamental Constants (AMCO-7), Ed. O. Klepper, Darmstadt (1984), p. 661.

57. N. Bendali, H.T. Duong, J.M. Saint Jalm, and J.L. Vialle, J. Physique (Paris) 44, 1019 (1983).

58. B. Fan, A. Lurio, and D. Grischkowsky, Phys. Rev. Lett. 41, 1460 (1978).

59. S.D. Rosner, T.D. Gaily, and R.A. Holt, Phys. Rev. Lett. 40, 851 (1978).

60. R.A. Holt, S.D. Rosner, T.D. Gaily, and A.G. Adam, Phys. Rev. A 22, 1563 (1980).

61. A.C. Mueller, F. Buchinger, W. Klempt, E.W. Otten, R. Neugart, C. Ekström, and J. Heinemeier, Nucl. Phys. A403, 234 (1983).

62. F. von Sichart, H.J. Stöckmann, H. Ackermann, and G. zu Putlitz, Z. Phys. 236, 97 (1970).

63. U. Nielsen, O. Poulsen, P. Thorsen, and H. Crosswhite, Phys. Rev. Lett. 51, 1749 (1983).

64. M. Van Hove, G. Borghs, P. De Bisschop, and R.E. Silverans, Z. Phys. A 321, 215 (1985).

65. U. Kötz, J. Kowalski, R. Neumann, S. Noehte, H. Suhr, K. Winkler, and G. zu Putlitz, Z. Phys. A 300, 25 (1981).

66. N. Bendali, H.T. Duong, J.M. Saint-Jalm, and J.L. Vialle, J. Physique 45, 421 (1984).

67. G. Borghs, P. De Bisschop, M. Van Hove, and R.E. Silverans, Phys. Rev. Lett. 52, 2030 (1984).

68. M. Carré, J. Lermé, and J.L. Vialle, J. Phys. B19, 2853 (1986).

69. F. Beguin, M.L. Gaillard, H. Winter, and G. Meunier, J. Physique (Paris) 38, 1185 (1977).

70. F. Beguin-Renier, J. Désesquelles, and M.L. Gaillard, Physica Scr. 18, 21 (1978).

71. U. Dinger, J. Eberz, G. Huber, H. Lochmann, and G. Ulm, Z. Phys. D1, 137 (1986).

72. O. Poulsen, P. Nielsen, U. Nielsen, P.S. Ramanujam, and N.I. Winstrup, Phys. Rev. A 27, 913 (1983).

73. M. Kaivola, P. Thorsen, and O. Poulsen, Phys. Rev. A 32, 207 (1985).

74. R.E. Silverans, P. De Bisschop, M. Van Hove, J.M. Van den Cruyce, and G. Borghs, Phys. Lett. 82A, 70 (1981).

75. G. Borghs, P. De Bisschop, J.-M. Van den Cruyce, M. Van Hove, and R.E. Silverans, Phys. Rev. Lett. 46, 1074 (1981).

76. M.L. Lewis and P.H. Serafino, Phys. Rev. A 18, 867 (1978).

77. B. Fan, D. Grischkowsky, and A. Lurio, Optics Letters 4, 233 (1979).

78. R. Bayer, J. Kowakski, R. Neumann, S. Noehte, H. Suhr, K. Winkler, and G. zu Putlitz, Z. Phys. A 292, 329 (1979).

79. A.N. Jette, T. Lee, and T.P. Das, Phys. Rev. A 9, 2337 (1974).

80. B. Schiff, Y. Accad, and C.L. Pekeris, Phys. Rev. A 8, 2272 (1973).

81. A.M. Ermolaev, Phys. Rev. A 8, 1651 (1973); Phys. Rev. Lett. 34, 380 (1975).

82. J. Kowalski, R. Neumann, S. Noehte, R. Schwarzwald, H. Suhr, and G. zu Putlitz, in Laser Spectroscopy VI, Eds. H.P. Weber and W. Lüthy, Springer, Berlin (1983) p. 40.

83. U. Kötz, J. Kowalski, R. Neumann, S. Noehte, H. Suhr, K. Winkler, and G. zu Putlitz, in Precision Measurement and Fundamental Constants II, Eds. B.N. Taylor and W.D. Phillips, Natl. Bur. Stand. (U.S.), Spec. Publ. 617 (1984), p. 159.

84. J. Kowalski, R. Neumann, S. Noehte, H. Suhr, G. zu Putlitz, and R. Herman, Acta Physica Hungarica 56, 199 (1984).

85. Ch.E. Moore, Atomic Energy Levels, Vol. 1 - 3, NSRDS-NBS 35, National Bureau of Standards, Washington (1971).

86. W.C. Martin, R. Zalubas, and L. Hagan, Atomic Energy Levels - The Rare-Earth Elements, NSRDS-NBS 60, National Bureau of Standards, Washington (1978).

87. O. Poulsen, T. Andersen, S.M. Bentzen, and U. Nielsen, Phys. Rev. A 24, 2523 (1981).

88. G. Huber, private communication.

89. H.T. Duong, P. Juncar, S. Liberman, A.C. Mueller, R. Neugart, E.W. Otten, B. Peuse, J. Pinard, H.H. Stroke, C. Thibault, F. Touchard, J.L. Vialle, and K. Wendt, Europhysics Letters 3, 175 (1987).

90. S. Liberman, J. Pinard, H.T. Duong, P. Juncar, J.L. Vialle, P. Jacquinot, G. Huber, F. Touchard, S. Büttgenbach, A. Pesnelle, C. Thibault, and R. Klapisch, C.R. Acad. Sci. (Paris) 286B, 253 (1978).

91. N. Bendali, H.T. Duong, P. Juncar, S. Liberman, J. Pinard, J.-M. Saint-Jalm, J.L. Vialle, S. Büttgenbach, C. Thibault, F. Touchard, A. Pesnelle, and A.C. Mueller, C.R. Acad. Sci. (Paris) 299 Ser. II, 1157 (1984).

92. H. Lundberg and A. Rosén, Z. Phys. A 286, 329 (1978).

93. V.A. Dzuba, V.V. Flambaum, and O.P. Sushkov, Phys. Lett. 95A, 230 (1983).

94. G. Borghs, P. De Bisschop, R.E. Silverans, M. Van Hove, and J.M. Van den Cruyce, Z. Phys. A 299, 11 (1981).

95. C.R. Bingham, M.L. Gaillard, D.J. Pegg, H.K. Carter, R.L. Mlekodaj, J.D. Cole, and P.M. Griffin, Nucl. Instr. Meth. 202, 147 (1982).

96. C. Höhle, H. Hühnermann, Th. Meier, and H. Wagner, Z. Phys. A 284, 261 (1978).
97. E. Alvarez, A. Arnesen, A. Bengtson, R. Hallin, M. Niburg, C. Nordling, and T. Noreland, Physica Scr. 18, 54 (1978).
98. M. Van Hove, G. Borghs, P. De Bisschop, and R.E. Silverans, J. Phys. B 15, 1805 (1982).
99. M. Wilson, Phys. Lett. 65A, 213 (1978).
100. R.E. Silverans, G. Borghs, P. De Bisschop, and M. Van Hove, Phys. Rev. A 33, 2117 (1986).
101. G. Borghs, P. De Bisschop, J. Odeurs, R.E. Silverans, and M. Van Hove, Phys. Rev. A 31, 1434 (1985).
102. K. Wendt, S.A. Ahmad, F. Buchinger, A.C. Mueller, R. Neugart, and E.W. Otten, Z. Phys. A 318, 125 (1984).
103. E. Rasmussen, Z. Phys. 86, 24 (1933); Z. Phys. 87, 607 (1934).
104. S.A. Ahmad, W. Klempt, R. Neugart, E.W. Otten, K. Wendt, and C. Ekström, Phys. Lett. 133B, 47 (1983).
105. K. Wendt, S.A. Ahmad, W. Klempt, R. Neugart, E.W. Otten, and H.H. Stroke, Z. Phys. D4, 227 (1987).
106. A. Lurio, Phys. Rev. 142, 46 (1966).
107. P.G.H. Sandars and J. Beck, Proc. Roy. Soc. A 289, 97 (1965).
108. J.L. Heully and A.M. Martensson-Pendrill, Physica Scr. 31, 169 (1985).
109. V.A. Dzuba, V.V. Flambaum, and O.P. Sushkov, Physica Scr. 32, 507 (1985).
110. T.P. Das, private communication and to be published.
111. G. Torbohm, B. Fricke, and A. Rosén, Phys. Rev. A 31, 2038 (1985).
112. A. Arnesen, A. Bengtson, R. Hallin, C. Nordling, Ö. Staaf, and L. Ward, Physica Scr. 24, 747 (1981).
113. H. Schüler and Th. Schmidt, Z. Phys. 94, 457 (1935).
114. C. Höhle, H. Hühnermann, and H. Wagner, Z. Phys. A 304, 279 (1982).
115. J. Bauche, J.-F. Wyart, Z. Ben Ahmed, and K. Guidara, Z. Phys. A 304, 285 (1982).

116. C. Höhle, H. Hühnermann, and M. Elbel, Z. Phys. A 295, 1 (1980).
117. A. Bengtson, E. Alvarez, A. Arnesen, R. Hallin, C. Nordling, and Ö. Staaf, Phys. Lett. 76A, 45 (1980).
118. A. Arnesen, R. Hallin, C. Nordling, Ö. Staaf, L. Ward, B. Jelénković, M.Kisielinski, L. Lundin, and S. Mannervik, Astron. Astrophys. 106, 327 (1982).
119. A. Eichhorn, M. Elbel, W. Kamke, and J.C. Amaré, Opt. Commun. 31, 306 (1979).
120. A. Eichhorn, M. Elbel, W. Kamke, R. Quad, and J. Bauche, Z. Phys. A 305, 39 (1982).
121. A. Eichhorn, M. Elbel, W. Kamke, R. Quad, and H.J. Seifner, Physica 124C, 282 (1984).
122. E.W. Otten, Nucl. Phys. A 354, 471c (1981).
123. H.L. Ravn, Phys. Reports 54, 201 (1979).
124. H. Kopfermann, Nuclear Moments, Academic Press, New York (1958).
125. H.G. Kuhn, Atomic Spectra, Longman, London (1969).
126. K. Heilig and A. Steudel, At. Data Nucl. Data Tables 14, 613 (1974).
127. H.-J. Kluge, Hyperfine Interactions 24-26, 69 (1985).
128. C. Thibault, Hyperfine Interactions 24-26, 95 (1985).
129. H. Lochmann, U. Dinger, J. Eberz, G. Huber, R. Menges, G. Ulm, R. Kirchner, O. Klepper, T. Kühl, D. Marx, and D. Schardt, Z. Phys. A 322, 703 (1985).
130. J. Eberz, U. Dinger, T. Horiguchi, G. Huber, H. Lochmann, R. Menges, R. Kirchner, O. Klepper, T. Kühl, D. Marx, E. Roeckl, and D. Schardt, Z. Phys. A 323, 119 (1986)
131. J. Eberz, U. Dinger, G. Huber, H. Lochmann, R. Menges, R. Neugart, R. Kirchner, O. Klepper, T. Kühl, D. Marx, G. Ulm, and K. Wendt, Nucl. Phys. A 464, 9 (1987).
132. J. Eberz, U. Dinger, G. Huber, H. Lochmann, R. Menges, G. Ulm, R. Kirchner, O. Klepper, T. Kühl, D. Marx, and D. Schardt, Z. Phys. A 326, 121 (1987).
133. J. Bonn, W. Klempt, R. Neugart, E.W. Otten, and B. Schinzler, Z. Phys. A 289, 227 (1979).

134. R. Neugart, F. Buchinger, W. Klempt, A.C. Mueller, E.W. Otten, C. Ekström, and J. Heinemeier, Hyperfine Interactions 9, 151 (1981).

135. R.E. Silverans, G. Borghs, and J.-M. Van den Cruyce, Hyperfine Interactions 9, 193 (1981).

136. K. Dörschel, H. Hühnermann, E. Knobl, Th. Meier, and H. Wagner, Z. Phys. A 302, 359 (1981).

137. G.D. Alkhazov, E.Ye. Berlovich, V.P. Denisov, W. Heddrich, H. Hühnermann, E.W. Peau, and H. Wagner, Proc. 7th Int. Conf. on Atomic Masses and Fundamental Constants (AMCO-7), Ed. O. Klepper, Darmstadt (1984), p. 327.

138. K. Dörschel, W. Heddrich, H. Hühnermann, E.W. Peau, H. Wagner, G.D. Alkhazov, E.Ye. Berlovich, V.P. Denisov, V.N. Panteleev, and A.G. Polyakov, Z. Phys. A 312, 269 (1983).

139. K. Dörschel, W. Heddrich, H. Hühnermann, E.W. Peau, H. Wagner, G.D. Alkhazov, E.Ye. Berlovich, V.P. Denisov, V.N. Panteleev, and A.G. Polyakov, Z. Phys. A 317, 233 (1984).

140. G.D. Alkhazov, E.Ye. Berlovich, V.P. Denisov, V.N. Panteleev, V.I. Tikhonov, K. Dörschel, W. Heddrich, H. Hühnermann, E.W. Peau, and H. Wagner, Z. Phys. A 316, 123 (1984).

141. S.A. Ahmad, W. Klempt, C. Ekström, R. Neugart, and K. Wendt, Z. Phys. A 321, 35 (1985).

142. S.A. Ahmad, C. Ekström, W. Klempt, R. Neugart, and K. Wendt, Proc. 7th Int. Conf. on Atomic Masses and Fundamental Constants (AMCO-7), Ed. O. Klepper, Darmstadt (1984), p. 341.

143. R. Neugart, in Lasers in Nuclear Physics, Eds. C.E. Bemis, jr., and H.K. Carter, Nuclear Science Research Conference Series, Vol. 3, p. 231, Harwood, Chur, London, New York (1982).

144. R. Neugart, K. Wendt, S.A. Ahmad, W. Klempt, and C. Ekström, Hyperfine Interactions, 15/16, 181 (1983).

145. W. Klempt, R. Neugart, F. Buchinger, A.C. Mueller, K. Wendt, and C. Ekström, submitted to Z. Phys. A.

146. S.A. Ahmad, C. Ekström, W. Klempt, R. Neugart, and K. Wendt, to be published.

147. G. Ulm, S.K. Bhattacherjee, P. Dabkiewicz, G. Huber, H.-J. Kluge, T. Kühl, H. Lochmann, E.W. Otten, K. Wendt, S.A. Ahmad, W. Klempt, and R. Neugart, Z. Phys. A 325, 247 (1986).

148. R. Neugart, H.H. Stroke, S.A. Ahmad, H.T. Duong, H.L. Ravn, and K. Wendt, Phys. Rev. Lett. 55, 1559 (1985).

149. J.A. Bounds, C.R. Bingham, P. Juncar, H.K. Carter, G.A. Leander, R.L. Mlekodaj, E.H. Spejewski, and W.M. Fairbank, jr., Phys. Rev. Lett. 55, 2269 (1985).

150. R. Neugart, E.W. Otten, H.T. Duong, G. Ulm, and K. Wendt, European Conference Abstracts (2'ECAMP, Amsterdam) 9B, 15 (1985).

151. G. Ulm, H.T. Duong, K. Wendt, W. Borchers, R. Neugart, E.W. Otten, to be published.

152. S.A. Ahmad, C. Ekström, W. Klempt, R. Neugart, E.W. Otten, and K. Wendt, Proc. 7th Int. Conf. on Atomic Masses and Fundamental Constants (AMCO-7), Ed. O. Klepper, Darmstadt (1984), p. 361.

153. S.A. Ahmad, C. Ekström, W. Klempt, R. Neugart, E.W. Otten, G. Ulm, and K. Wendt, submitted to Nucl. Phys. A.

154. K.-H. Georgi, Nucl. Instr. Meth. 186, 271 (1981).

155. G.A. Leander and R.K. Sheline, Nucl. Phys. A413, 375 (1984).

156. I. Ragnarsson, Phys. Lett. 130B, 353 (1983).

157. A. Arima and H. Hyuga, in Mesons in Nuclei, Eds. M. Rho and D.H. Wilkinson, North-Holland, Amsterdam (1979), p. 683.

158. M. Ogawa, R. Broda, K. Zell, P.J. Daly, and P. Kleinheinz, Phys. Rev. Lett. 41, 289 (1978).

159. P. Dabkiewicz, F. Buchinger, H. Fischer, H.-J. Kluge, H. Kremmling, T. Kühl, A.C. Mueller, and H.A. Schüssler, Phys. Lett. 82B, 199 (1979).

160. I. Ragnarsson, in Future Directions in Studies of Nuclei Far from Stability, Proc. Int. Symp. Nashville 1979, Eds. J.H. Hamilton, E.H. Spejewski, C.R. Bingham, and E.F. Zganjar, North-Holland, Amsterdam (1980), p. 367.

161. C. Ekström, in Proc. 4th Int. Conf. on Nuclei Far from Stability, Helsingör 1981, Eds. P.G. Hansen and O.B. Nielsen, CERN 81-09, Geneva (1981), p. 12.

162. W.D. Myers, Phys. Lett. 30B 451 (1969).

163. W.D. Myers and K.H. Schmidt, Nucl. Phys. A410, 61 (1983).

164. A.N. Zherikhin, O.N. Kompanets, V.S. Letokhov, V.I. Mishin, V.N. Fedoseev, G.D. Alkhazov, A.E. Barzakh, E.E. Berlovich, V.P. Denisov, A.G. Dernyatin, and V.S. Ivanov, Zh. Eksp. Teor. Fiz. 86, 1249 (1984) [English transl. Sov. Phys. JETP 59, 729 (1984)].

165. V.N. Fedoseev, V.S. Letokhov, V.I. Mishin, G.D. Alkhazov, A.E. Barzakh, V.P. Denisov, A.g. Dernyatin, and V.S. Ivanov, Opt. Commun. 52, 24 (1984).

166. P. Brix and H. Kopfermann, Z. Phys. 126, 344 (1949).

167. P. Brix and H. Kopfermann, Rev. Mod. Phys. 30, 517 (1958).

168. A. Coc, C. Thibault, F. Touchard, H.T. Duong, P. Juncar, S. Liberman, J. Pinard, J. Lermé, J.L. Vialle, S. Büttgenbach, A.C. Mueller, and A. Pesnelle, Phys. Lett. 163B, 66 (1985).

169. R.K. Sheline, D. Decman, K. Nybø, T.F. Thorsteinsen, G. Løvhøiden, E.R. Flynn, J.A. Cizewski, D.K. Burke, G. Sletten, P. Hill, N. Kaffrell, W. Kurcewicz, G. Nyman, and G. Leander, Phys. Lett. 133B, 13 (1983).

170. G.S. Hurst, M.G. Payne, S.D. Kramer, and J.P. Young, Rev. Mod. Phys. 51, 767 (1979).

171. V.I. Balykin, G.I. Bekov, V.S. Letokhov, and V.I. Mishin, Usp. Fiz. Nauk 132, 293 (1980) [English transl. Sov. Phys. Usp. 23, 651 (1980)].

172. Yu. A. Kudryavtsev, V.S. Letokhov, and V.V. Petrunin, Pis'ma Zh. Eksp. Teor. Fiz. 42, 23 (1985) [English transl. JETP Letters 42, 26 (1985)].

173. N. Bendali, H.T. Duong, P. Juncar, J.K.P. Lee, J.M. Saint-Jalm, and J.L. Vialle, J. Phys. (Paris) 47, 1167 (1986).

174. R.E. Silverans, G. Borghs, P. De Bisschop, and M. Van Hove, Hyperfine Interactions 24-26, 181 (1985).

175. R. Neugart, Hyperfine Interactions 24-26, 159 (1985).

176. R. Neugart, W. Klempt, and K. Wendt, Nucl. Instr. Meth. B 17, 354 (1986).

177. E.W. Otten, Hyperfine Interactions 21, 43 (1985).

178. E. Arnold, D. Bauer, J. Bonn, R. Gegenwart, T. Reichelt, and K.P.C. Spath, to be published.

179. E. Arnold, J. Bonn, R. Gegenwart, W. Neu, R. Neugart, E.W. Otten, G. Ulm, and K. Wendt, to be published.

180. J. Javanainen, M. Kaivola, U. Nielsen, O. Poulsen, and E. Riis, J. Opt. Soc. Am. B2, 1768 (1985).

181. G. Huber, private communication.

Figure Captions

Fig. 1 : Schematic set-up for collinear laser spectroscopy: a) The superimposed laser and ion beams pass through the interaction and fluorescence detection region at a variable potential. b) Neutralized beams are post-accelerated or decelerated by a potential at the charge-exchange cell. The beams may travel either in the same or in opposite directions.

Fig. 2 : Energy-loss spectrum of neutralized Cs atoms, on top of the hyperfine structure of ^{133}Cs ($6s\ ^2S_{1/2} - 7p\ ^2P_{3/2}$), for different Cs-vapour pressures in the charge-exchange cell: (1) resonant charge transfer, (2) non-resonant charge transfer and collisional excitation 6s-6p, (3) and (4) multiple excitation 6s-6p.

Fig. 3 : Excitation scheme for resonant two-photon spectroscopy on Ne I with a beam energy of 119.141 keV (from ref. 47).

Fig. 4 : Two-photon resonance in Ne I, detected in the decay 4d'-3p. The upper part shows the detuning of the intermediate level from the resonance condition as a function of the post-acceleration voltage (from ref. 47).

Fig. 5 : Experimental set-up for fast-beam laser-rf double resonance spectroscopy (from ref. 64).

Fig. 6 : Fluorescence signal versus static magnetic field applied between the optical pumping and detection regions, from the D 1 transition $^2S_{1/2}$, F = 2 - $^2P_{1/2}$, F' = 1 in Na I. The relative contributions of the single and double Larmor frequency, ω_L and $2\omega_L$, depend on the angle β between the alignment axis and the observation (from ref. 66).

Fig. 7 : V and Λ configurations for resonant three-level saturation spectroscopy (from ref. 72).

Fig. 8 : Saturation signal for the V configuration in Ne I, with the broad Doppler profile shifted by different post-acceleration voltages around the exact resonance at 61.763 keV (from ref. 72).

Fig. 9 : Chart of the nuclides with optically investigated chains of unstable isotopes marked by solid frames. Techniques other than collinear laser spectroscopy (see Table 1) were applied (partly) for Na, K, Ca, (Rb), Sr, Cd, (Sn), (Cs), (Ba), (Hg), Pb, and (Fr).

Fig. 10 : Essential components of the ISOLDE set-up for collinear fast-beam laser spectroscopy. The post-acceleration and scanning voltage on the charge-exchange cell ranges from +10 to -10 kV.

Fig. 11 : Hyperfine structure pattern of ^{151}Dy (I = 7/2) in the strong resonance transition at 4212 Å, with the resonances of the stable doubly-even isotopes ^{156,158}Dy in a common voltage scale for measuring the isotope shift. The linewidth of 60 MHz includes some power broadening.

Fig. 12 : Yield curve of Ra isotopes from ISOLDE, and $7s^2\ ^1S_0 - 7s7p\ ^1P_1$ resonances from the strongest and weakest beams of isotopes. ^{232}Ra was observed here for the first time. ^{220}Ra has the shortest half-life of 20 ms and $^{215-219}$Ra are too short-lived to diffuse out of the UC_2 target.

Fig. 13 : Nuclear magnetic dipole (μ) and electric quadrupole (Q_s) moments in the sequence of $5/2^+$ ground states of $^{141-155}$Eu.

Fig. 14 : Nilsson diagram for odd neutrons close to N = 82. The Fermi levels for N = 83, 85, and 87 indicate a successive filling of the $f_{7/2}$ shell. On the right, the experimental magnetic dipole and electric quadrupole moments are compared with the results from particle-rotor calculations assuming deformations of ε = 0.10 and 0.15. The trend of the quadrupole moments reproduces the increase of coupling to the collective motion, while the discrepancy in the trend for the magnetic moments is understood as a change of core polarization.

Fig. 15 : Change of mean square charge radii $\delta\langle r^2\rangle$ in the isotopic chain $^{140-153}$Eu as a function of neutron number N, with ^{145}Eu (N = 82) taken as reference point. The change in deformation $\delta\langle\beta^2\rangle^{1/2}$, with respect to N = 82, is indicated by the parallel lines, the slope of which is given by the droplet model.

Fig. 16 : Differences in the nuclear mean square charge radii between even isotopes of neutron numbers N - 2 and N (Brix-Kopfermann diagram) for the rare-earth region. The curve for Dy is similar to those for Nd, Sm, and Gd which also show the peak from the sudden onset of deformation at N = 90. This effect disappears in the lighter and heavier elements. Data points above (below) the dashed droplet model line indicate increasing (decreasing) deformation from N - 2 to N, and the reversal of this effect is due to the N = 82 shell closure.

Fig. 17 : Differences of mean square charge radii and odd-even staggering in Ra. The upper curve corresponds to the plot of Fig. 16. The lower curve represents the changes between neighbouring isotopes with full dots (open circles) for the steps from odd to even (even to odd) neutron number.

Fig. 18 : King plot of the 4683 Å line in Ra II against the 4826 Å line in Ra I. The inlays show the error bars enlarged by a factor of 100.

Fig. 19 : Simplified energy-level diagram of Kr I and the resonance $5s\,[3/2]_2 - 5p\,[3/2]_2$ in ^{84}Kr detected by fluorescence as well as state-selective collisional ionization of Kr atoms in the metastable state.

Table 1: Measurements on radioactive nuclides by collinear fast-beam laser spectroscopy.

Element	stable isotopes	investigated radioactive isotopes	production reactions	production facility	transition	wave-length (Å)	refer-ence
Rb I	85,87	89-93	$^{235}U(n_{th},fission)$	Mainz reactor	$5s\ ^2S_{1/2}-6p\ ^2P_{3/2}$	4202	51
In I	113,115	104-111	$^{92-100}Mo(^{16}O,pxn)$	GSI	$5p\ ^2P_{3/2}-6s\ ^2S_{1/2}$	4511	129,130
		111-127	$^{238}U(p,fission)$	ISOLDE	$5p\ ^2P_{1/2}-$	4102	131
Sn I	112,114-120, 122,124	108-111	$^{98-100}Mo(^{16}O,xn)$	GSI	$5p^2\ ^1S_0-5p6s\ ^1P_1$	4525	132
					$^3P_1$	5632	
Cs I	133	137-142	$^{235}U(n_{th},fission)$	Mainz reactor	$6s\ ^2S_{1/2}-7p\ ^2P_{3/2}$	4555	50,133
Ba I	130,132, 134-138	122,123,125,127, 131,137	$^{139}La(p,spallation)$	ISOLDE	$6s^2\ ^1S_0-6s6p\ ^1P_1$	5535	134,61
		139-146	$^{238}U(p,fission)$				
Ba II		140	radioactive source	Leuven	$5d\ ^2D_{3/2}-6p\ ^2P_{3/2}$	5854	135
		139-146,148	$^{238}U(p,fission)$	ISOLDE	$6s\ ^2S_{1/2}-6p\ ^2P_{3/2}$	4554	(see 61)
Sm II	144,147-150, 152,154	146,151	Sm(n capture)	LNPI Gat-china/Mol	$4f^65d\ ^8H_{17/2}-4f^66p;\ 15/2$	6569	136,137
Eu I	151,153	140-150,152	$^{181}Ta(p,spallation)$	ISOLDE	$4f^76s^2\ ^8S_{7/2}-4f^76s6p\ ^8P_{7/2}$	4627	141,142
		142-150			$^8P_{9/2}$	4594	
Eu II		147,149,152, 154-156	$^{181}Ta(p,spallation)$, Sm,Eu(n capture)	LNPI Gatchina	$4f^75d\ ^9D_4-4f^76p(7/2,3/2)_4$	6049	137-140
Gd I	152,154-158, 160	142,144-151,153	$^{181}Ta(p,spallation)$	ISOLDE	$4f^75d6s^2\ ^9D_6-4f^75d6s6p;\ 7$	4226	144,145
Dy I	156,158, 160-164	146-155,157,159	$^{181}Ta(p,spallation)$	ISOLDE	$4f^{10}6s^2\ ^5I_8-4f^{10}6s6p(8,1)_9$	4212	143-145
Er I	162,164, 166-168,170	150-160(even)	$^{181}Ta(p,spallation)$	ISOLDE	$4f^{12}6s^2\ ^3H_6-4f^{11}5d6s^2;\ 5$	4409	143-145
		154-160(even)			$-4f^{12}6s6p(6,1)_7$	5827	
		152-161,163,165			$-4f^{12}6s6p(6,1)_5$	4151	
Yb I	168,170-174, 176	158-169	$^{181}Ta(p,spallation)$	ISOLDE	$6s^2\ ^1S_0-6s6p\ ^3P_1$	5556	27,143-145
		156-166(even)			$6s6p\ ^3P_2-6s7s\ ^3S_1$	7699	
Hg I	196,198-202, 204	182-198(even)	Pb(p,spallation)	ISOLDE	$6s6p\ ^3P_2-6s7s\ ^3S_1$	5461	147
Tl I	203,205	207	$^{232}Th(p,spallation)$ $^{219}Fr \rightarrow ^{207}Tl$	ISOLDE	$6p\ ^2P_{3/2}-7s\ ^2S_{1/2}$	5350	148
		189,191,193	$^{181}Ta(^{16}O,xn)$	UNISOR			149
Rn I	-	202-212,218-222	$^{232}Th(p,spallation)$	ISOLDE	$7s[3/2]_2-7p[5/2]_3$	7450	150,151
Fr I	-	212-213,220-221	$^{232}Th(p,spallation)$	ISOLDE	$7s\ ^2S_{1/2}-8p\ ^2P_{1/2}$	4325	89
					$^2P_{3/2}$	4225	
Ra I	-	208-214,220-230, 232	$^{238}U(p,spallation)$	ISOLDE	$7s^2\ ^1S_0-7s7p\ ^1P_1$	4826	104,105, 152,153
		212,214,222-226			$^3P_1$	7141	
		212,214,221-224,226			$7s7p\ ^3P_2-7s7d\ ^3D_3$	6446	
Ra II	-	208,210-214, 220-230	$^{238}U(p,spallation)$	ISOLDE	$7s\ ^2S_{1/2}-7p\ ^2P_{1/2}$	4683	

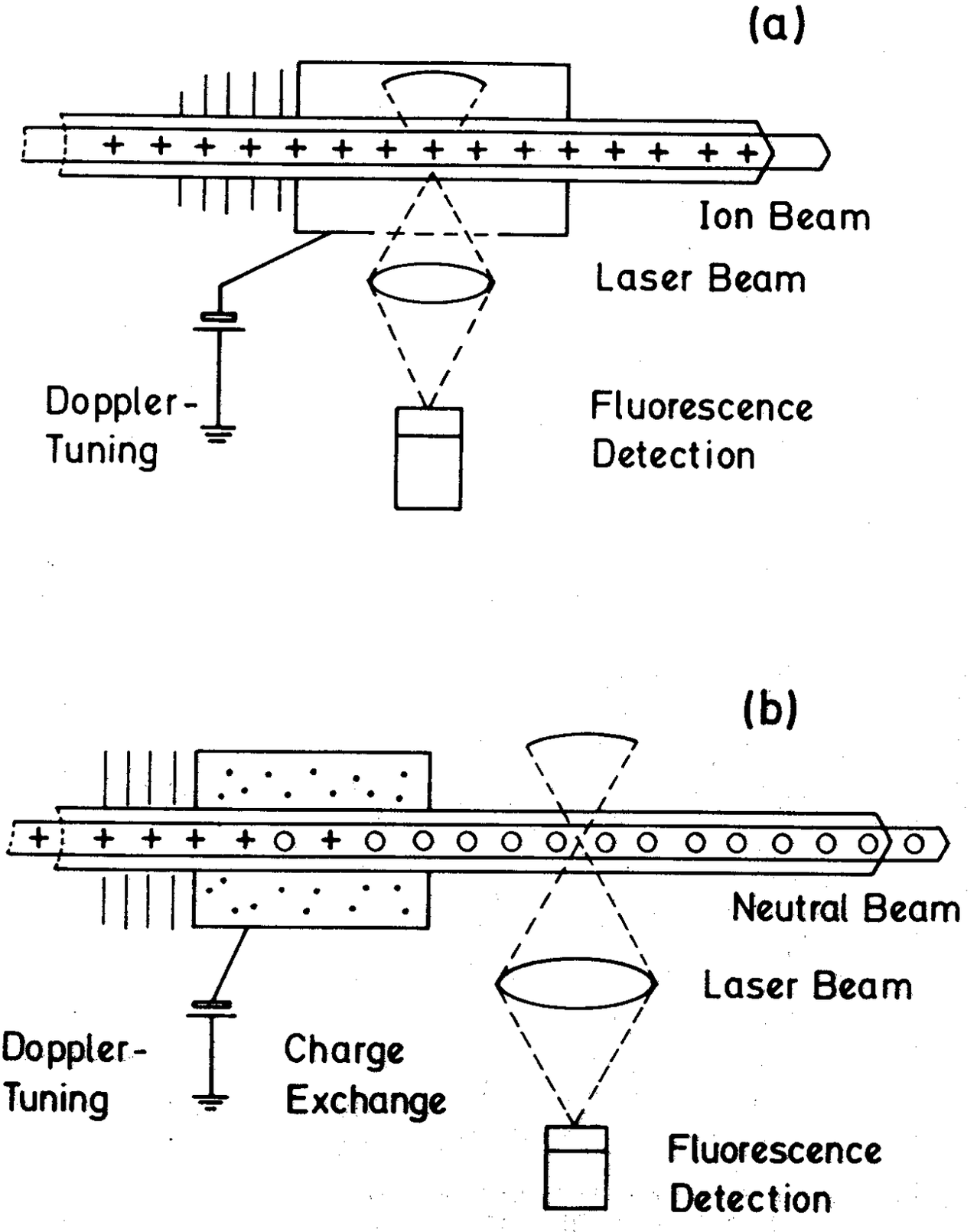
(a)
Ion Beam
Laser Beam
Doppler-
Tuning
Fluorescence
Detection
(b)
Neutral Beam
Laser Beam
Doppler-
Tuning
Charge
Exchange
Fluorescence
Detection

Fig. 1

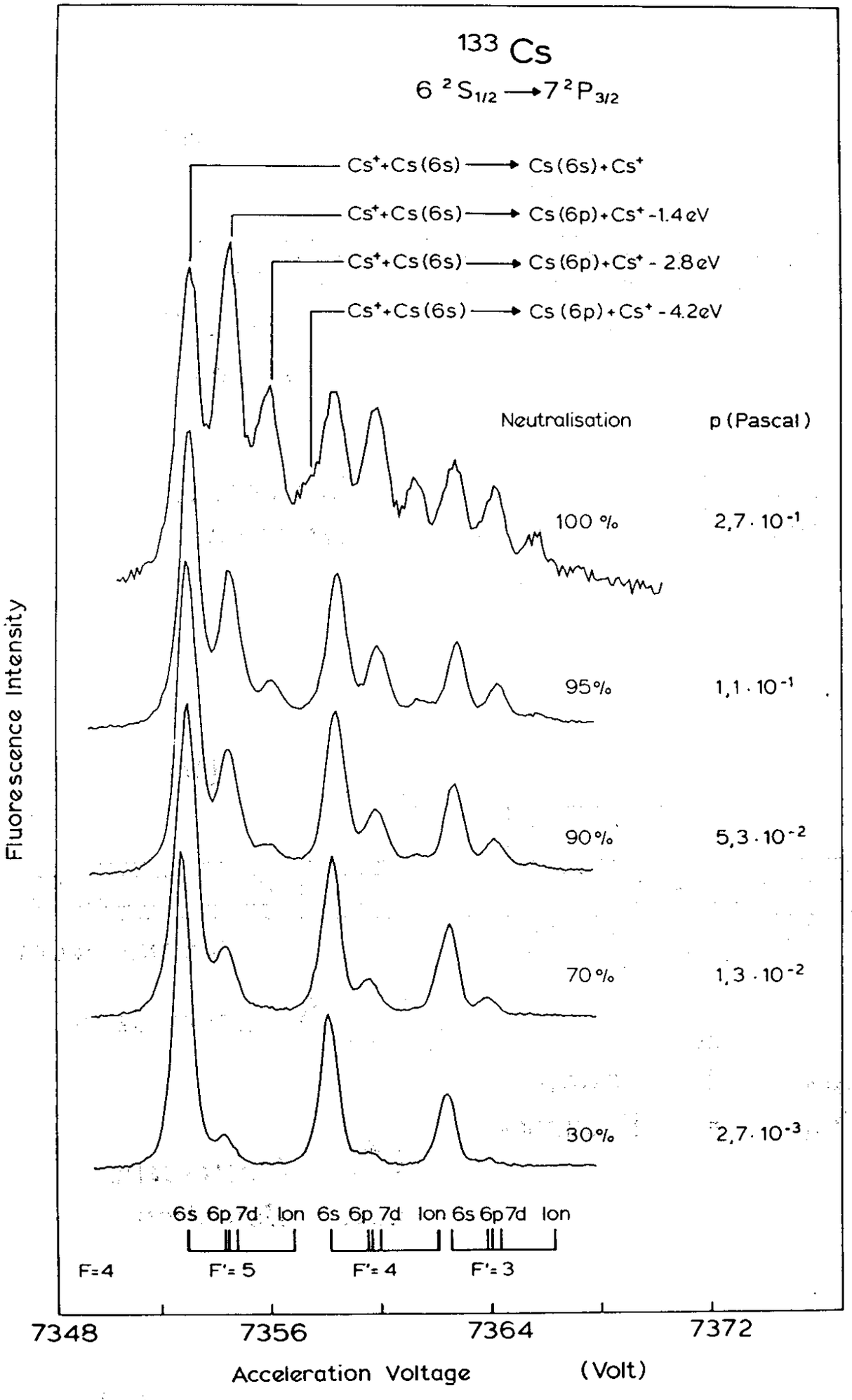
133 Cs
6 ²S1/2 → 7 ²P3/2
Cs⁺+Cs(6s) → Cs(6s)+Cs⁺
Cs⁺+Cs(6s) → Cs(6p)+Cs⁺ -1.4eV
Cs⁺+Cs(6s) → Cs(6p)+Cs⁺ - 2.8eV
Cs⁺+Cs(6s) → Cs(6p)+Cs⁺ - 4.2eV
Neutralisation
p (Pascal)
100 %
2,7 · 10⁻¹
95%
1,1 · 10⁻¹
90%
5,3 · 10⁻²
70%
1,3 · 10⁻²
30%
2,7 · 10⁻³
6s 6p 7d Ion 6s 6p 7d Ion 6s 6p 7d Ion
F=4
F'= 5
F'= 4
F'= 3
Fluorescence Intensity
7348
7356
7364
7372
Acceleration Voltage (Volt)

Fig. 2

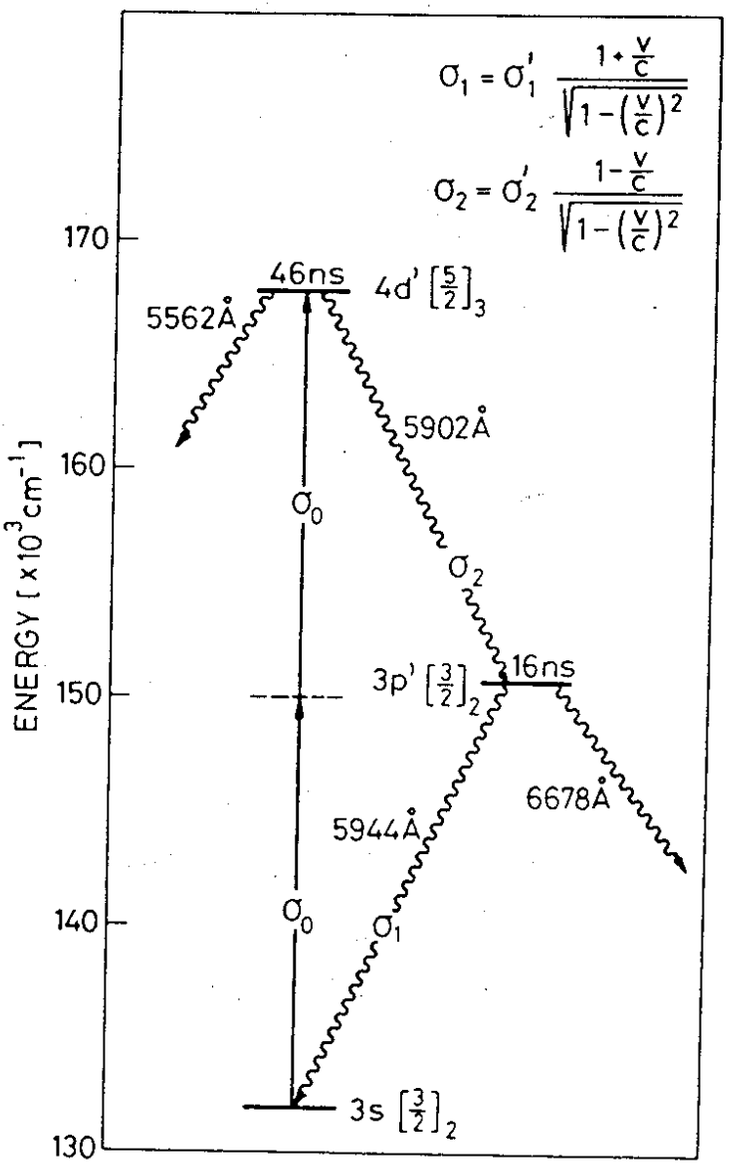
$\sigma_1 = \sigma_1' \frac{1+\frac{v}{c}}{\sqrt{1-(\frac{v}{c})^2}}$
$\sigma_2 = \sigma_2' \frac{1-\frac{v}{c}}{\sqrt{1-(\frac{v}{c})^2}}$
ENERGY [$\times 10^3 cm^{-1}$]
170
160
150
140
130
46ns
$4d' [\frac{5}{2}]_3$
5562Å
5902Å
σ_0
σ_2
$3p' [\frac{3}{2}]_2$
16ns
6678Å
5944Å
σ_0
σ_1
$3s [\frac{3}{2}]_2$

Fig. 3

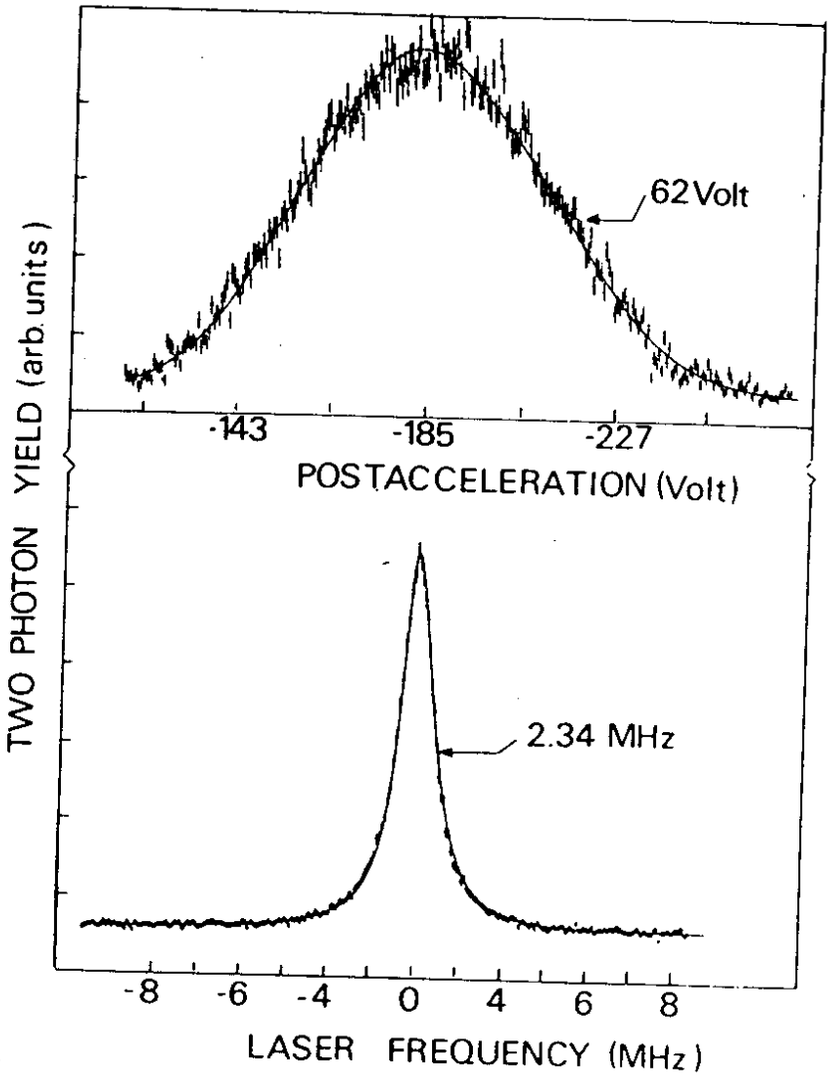
62Volt
-143
-185
-227
POSTACCELERATION (Volt)
TWO PHOTON YIELD (arb.units)
2.34 MHz
-8
-6
-4
0
4
6
8
LASER FREQUENCY (MHz)

Fig. 4

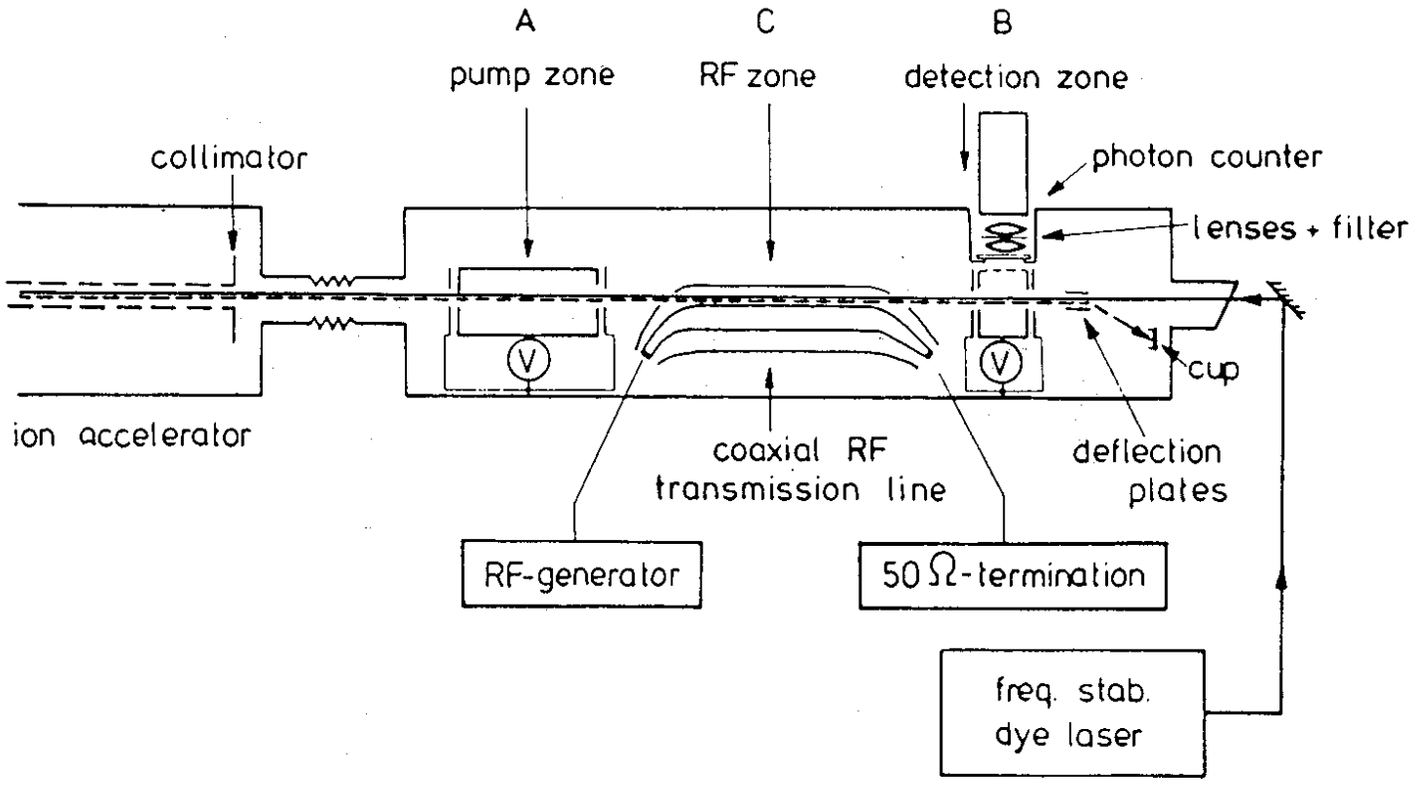
A
pump zone
C
RF zone
B
detection zone
collimator
photon counter
lenses + filter
V
V
cup
ion accelerator
coaxial RF
transmission line
deflection
plates
RF-generator
50 Ω-termination
freq. stab.
dye laser

Fig. 5

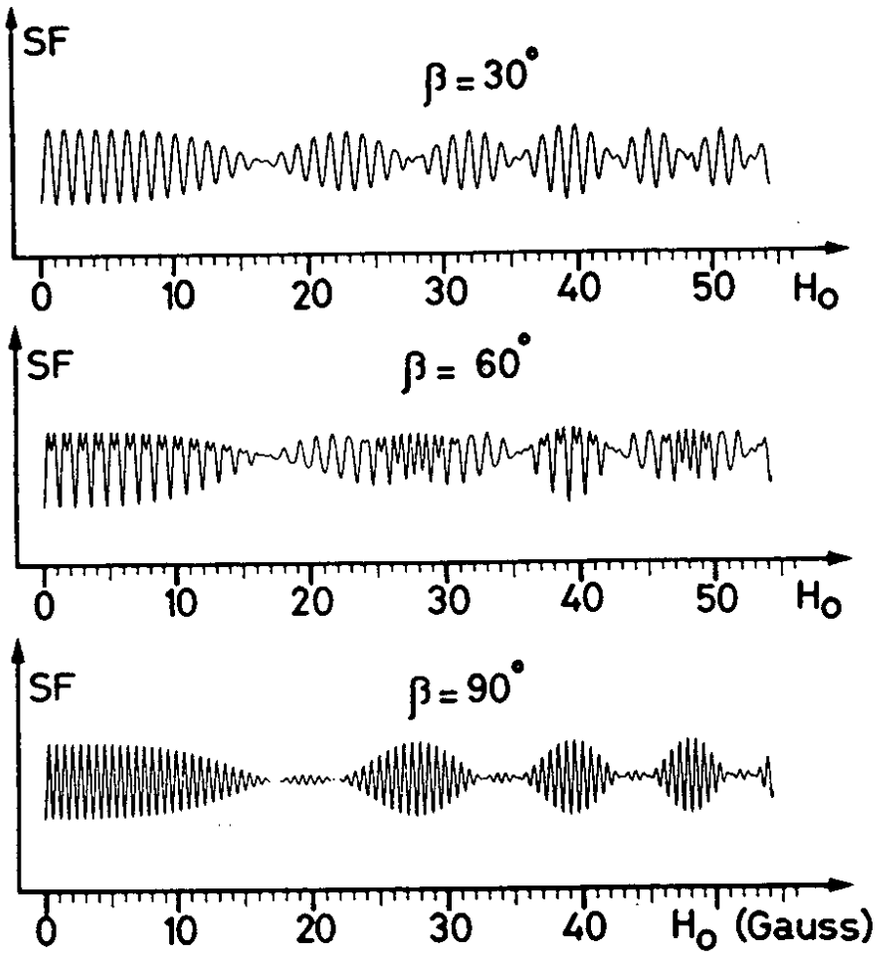
SF
β = 30°
0
10
20
30
40
50
Ho
SF
β = 60°
0
10
20
30
40
50
Ho
SF
β = 90°
0
10
20
30
40
Ho (Gauss)

Fig. 6

$$\sigma_1 = \sigma_L \gamma(\beta)(1-\beta)$$
$$\sigma_2 = \sigma_L \gamma(\beta)(1+\beta)$$

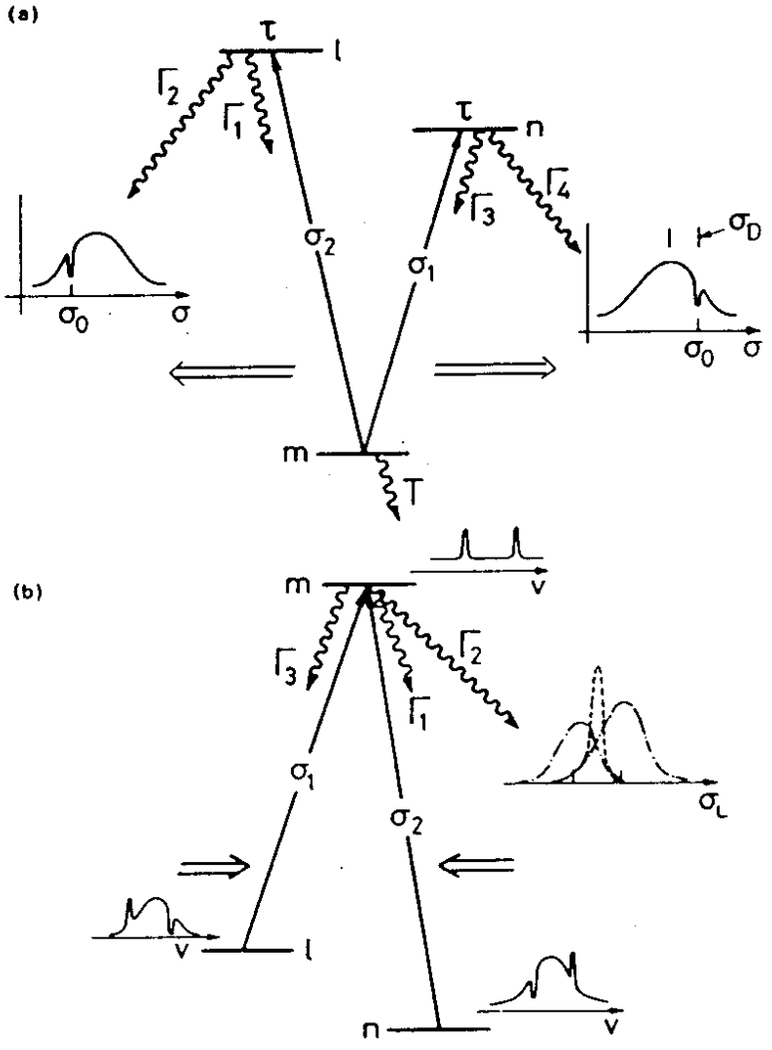

Fig. 7

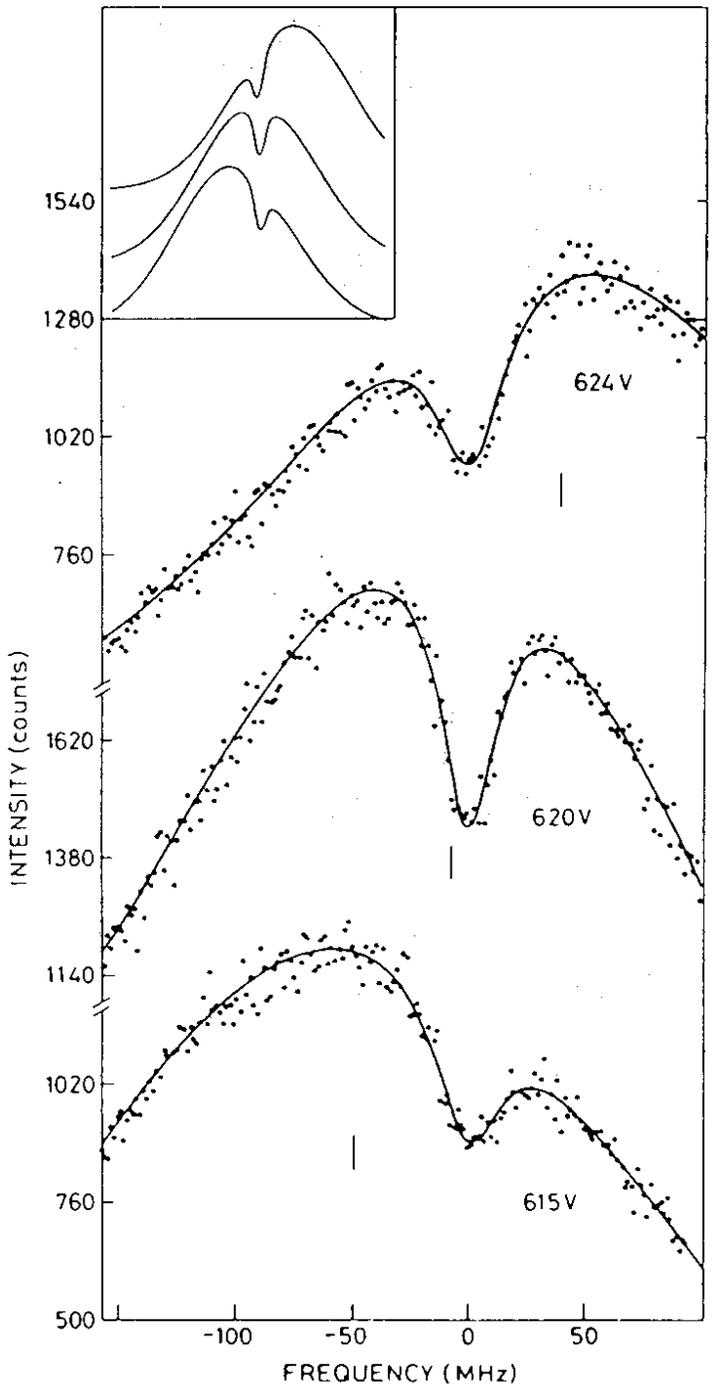
1540
1280
1020
760
624V
1620
1380
1140
620V
1020
760
615V
500
INTENSITY (counts)
-100
-50
0
50
FREQUENCY (MHz)

Fig. 8

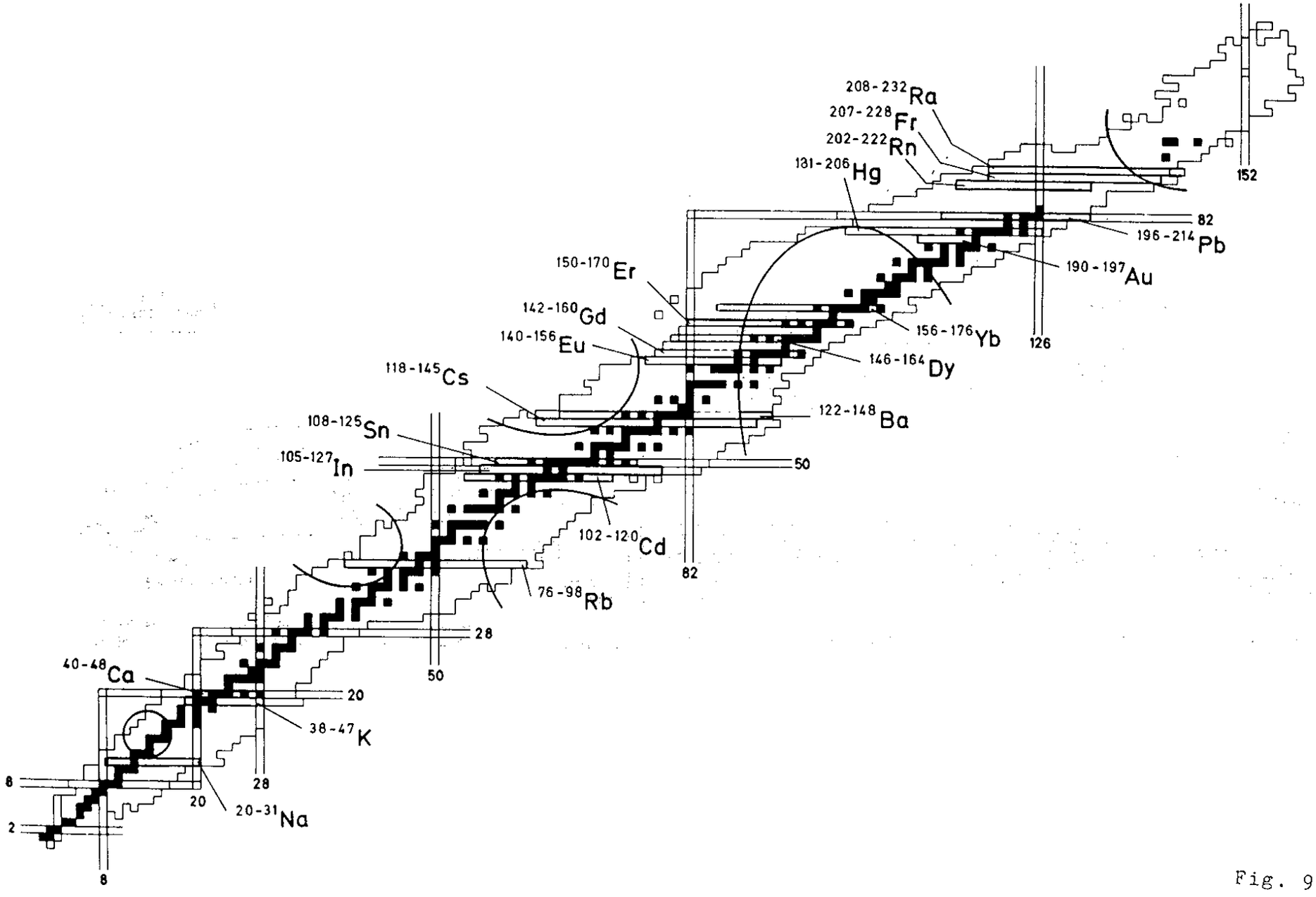
208-232Ra
207-228Fr
202-222Rn
131-206Hg
196-214Pb
190-197Au
156-176Yb
146-164Dy
150-170Er
142-160Gd
140-156Eu
118-145Cs
122-148Ba
108-125Sn
105-127In
102-120Cd
76-98Rb
40-48Ca
38-47K
20-31Na
152
126
82
50
28
20
8
2

Fig. 9

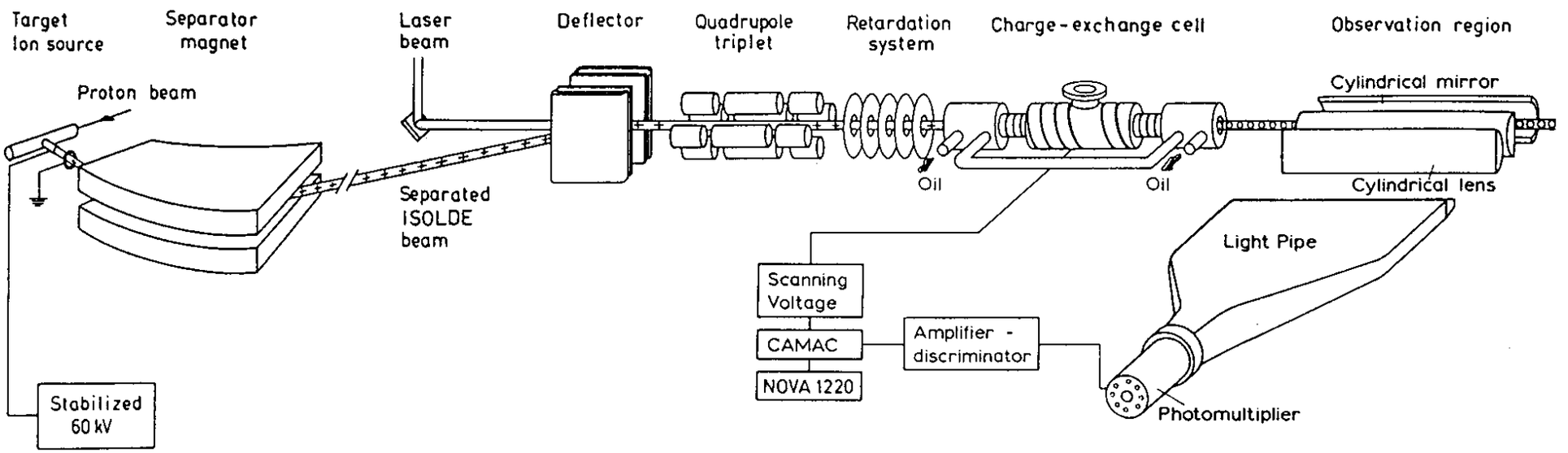
Target
Ion source
Separator
magnet
Laser
beam
Deflector
Quadrupole
triplet
Retardation
system
Charge-exchange cell
Observation region
Proton beam
Cylindrical mirror
Separated
ISOLDE
beam
Oil
Oil
Cylindrical lens
Light Pipe
Scanning
Voltage
CAMAC
NOVA 1220
Amplifier -
discriminator
Stabilized
60 kV
Photomultiplier

Fig. 10

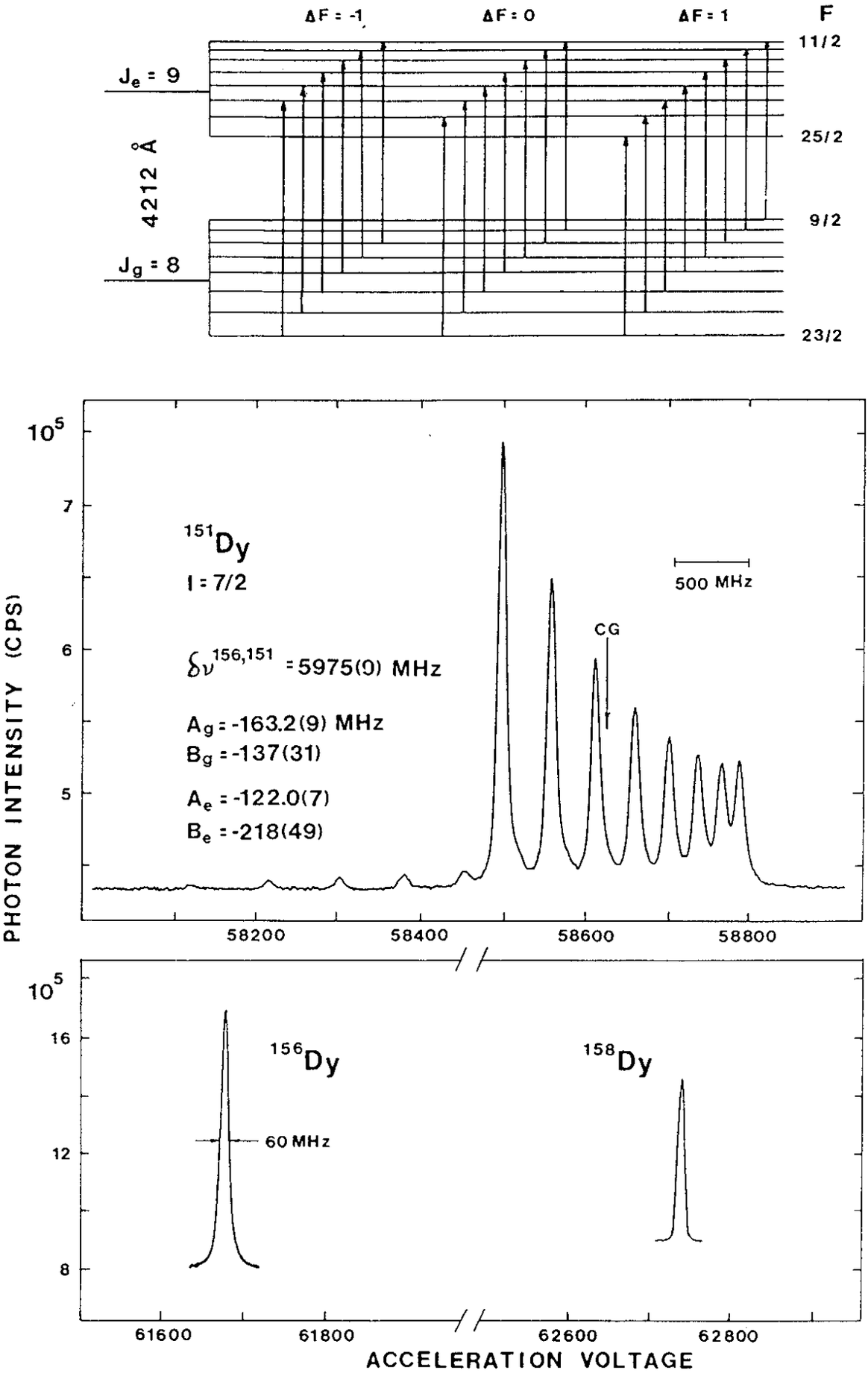
ΔF = -1
ΔF = 0
ΔF = 1
F
11/2
25/2
9/2
23/2
J_e = 9
J_g = 8
4212 Å
PHOTON INTENSITY (CPS)
10^5
7
6
5
^{151}Dy
I = 7/2
$\delta\nu^{156,151}$ = 5975(0) MHz
A_g = -163.2(9) MHz
B_g = -137(31)
A_e = -122.0(7)
B_e = -218(49)
500 MHz
CG
58200
58400
58600
58800
10^5
16
12
8
^{156}Dy
60 MHz
^{158}Dy
61600
61800
62600
62800
ACCELERATION VOLTAGE

Fig. 11

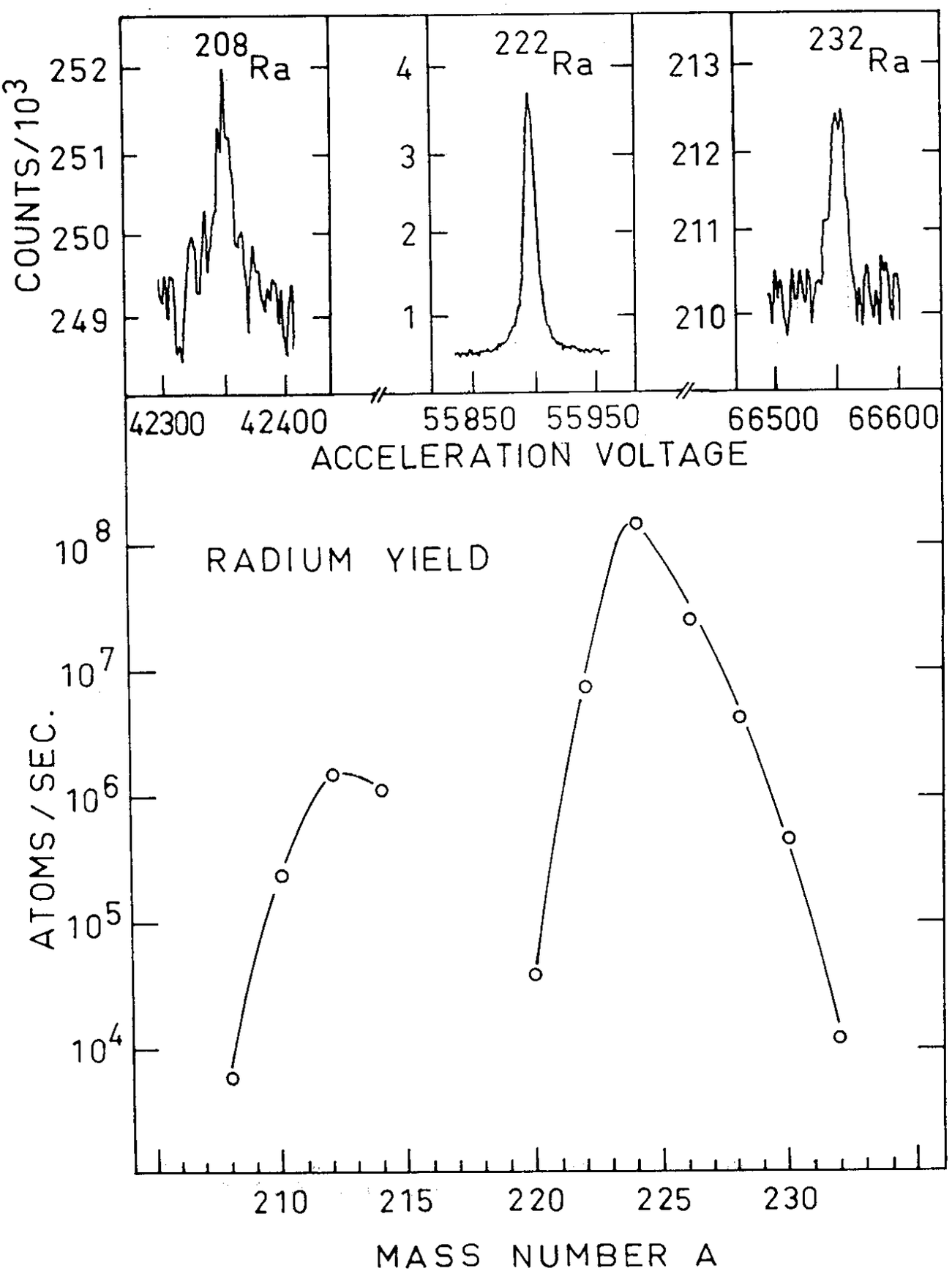
208Ra
222Ra
232Ra
COUNTS/10^3
252
251
250
249
4
3
2
1
213
212
211
210
42300
42400
55850
55950
66500
66600
ACCELERATION VOLTAGE
RADIUM YIELD
ATOMS / SEC.
10^8
10^7
10^6
10^5
10^4
210
215
220
225
230
MASS NUMBER A

Fig. 12

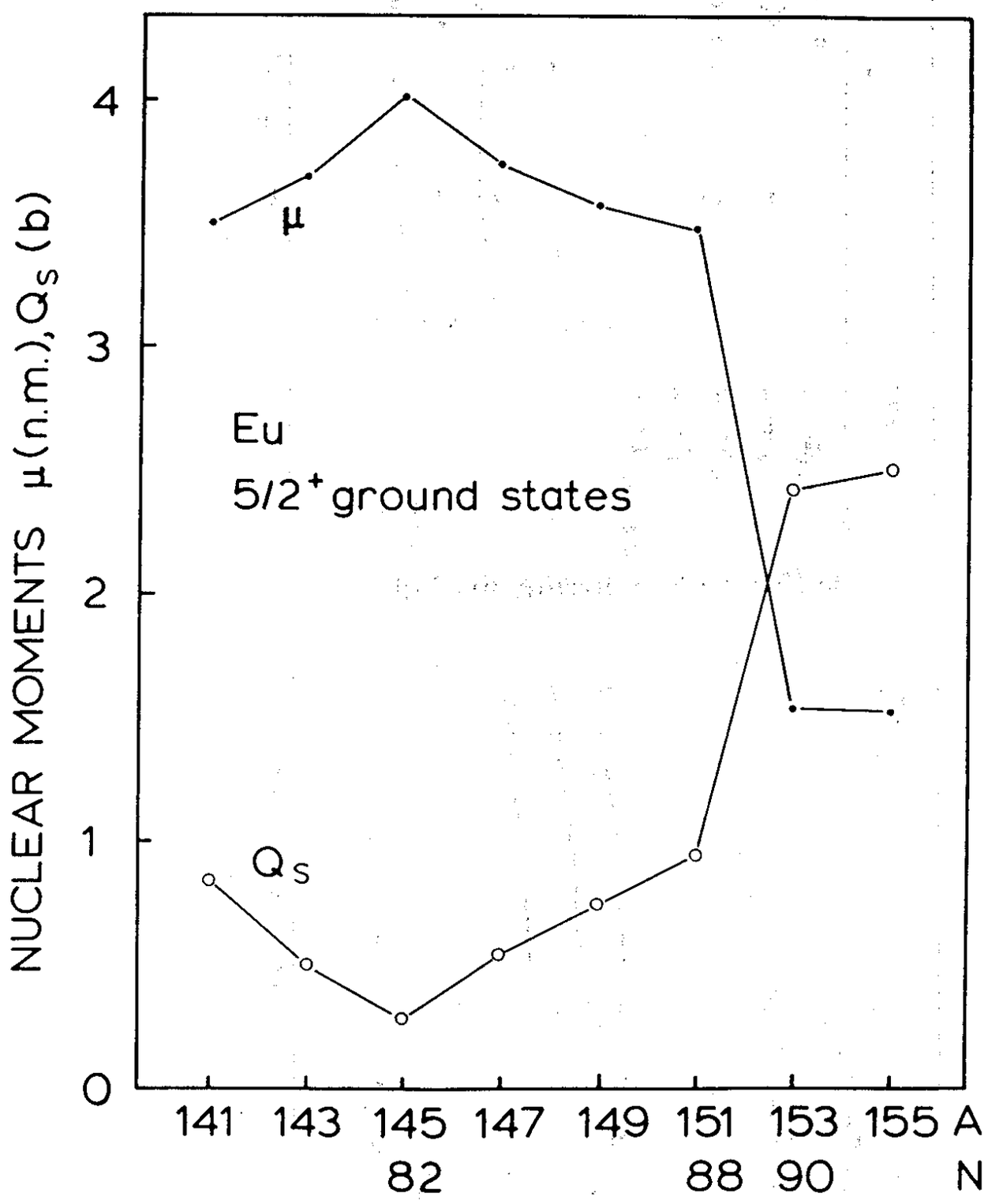
NUCLEAR MOMENTS μ(n.m.), Qs (b)
4
3
2
1
0
μ
Eu
5/2+ ground states
Qs
141
143
145
147
149
151
153
155
A
82
88
90
N

Fig. 13

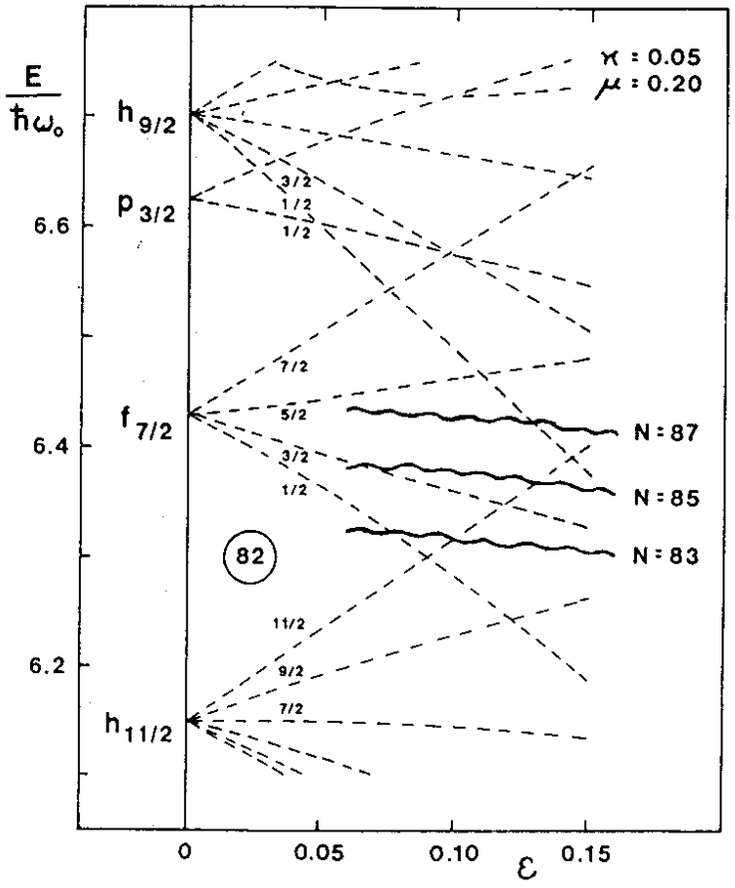
E / ħω₀
h9/2
p3/2
f7/2
h11/2
6.6
6.4
6.2
κ = 0.05
μ = 0.20
3/2
1/2
1/2
7/2
5/2
3/2
1/2
11/2
9/2
7/2
N = 87
N = 85
N = 83
82
0
0.05
0.10
0.15
ε

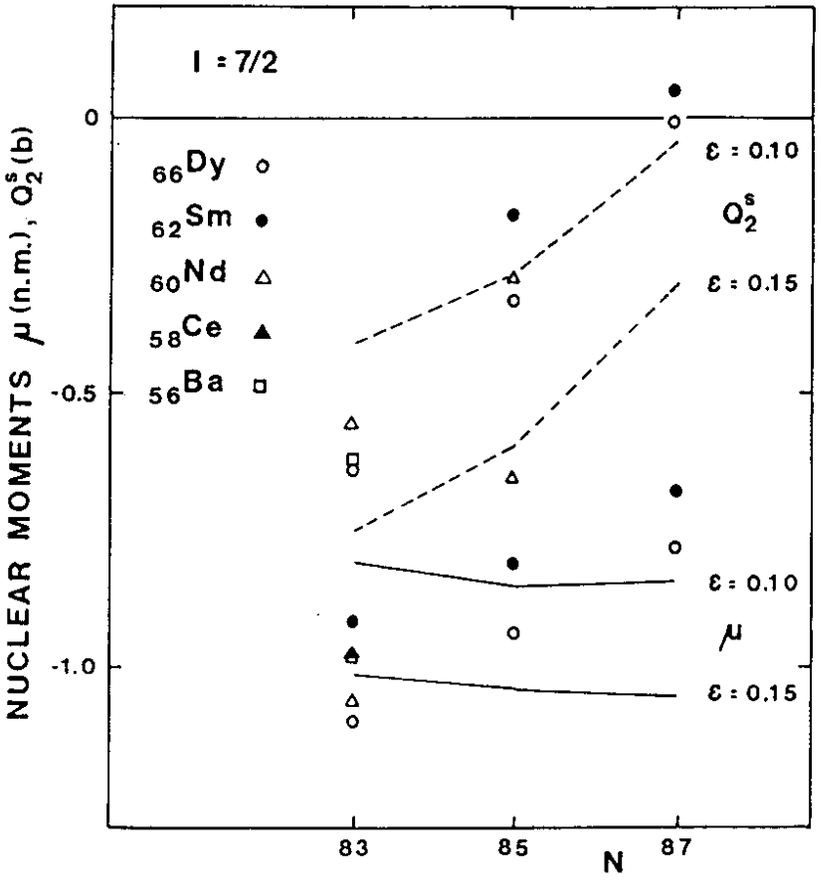
I = 7/2
NUCLEAR MOMENTS μ (n.m.), Q2s (b)
66Dy
62Sm
60Nd
58Ce
56Ba
0
-0.5
-1.0
ε = 0.10
Q2s
ε = 0.15
ε = 0.10
μ
ε = 0.15
83
85
87
N

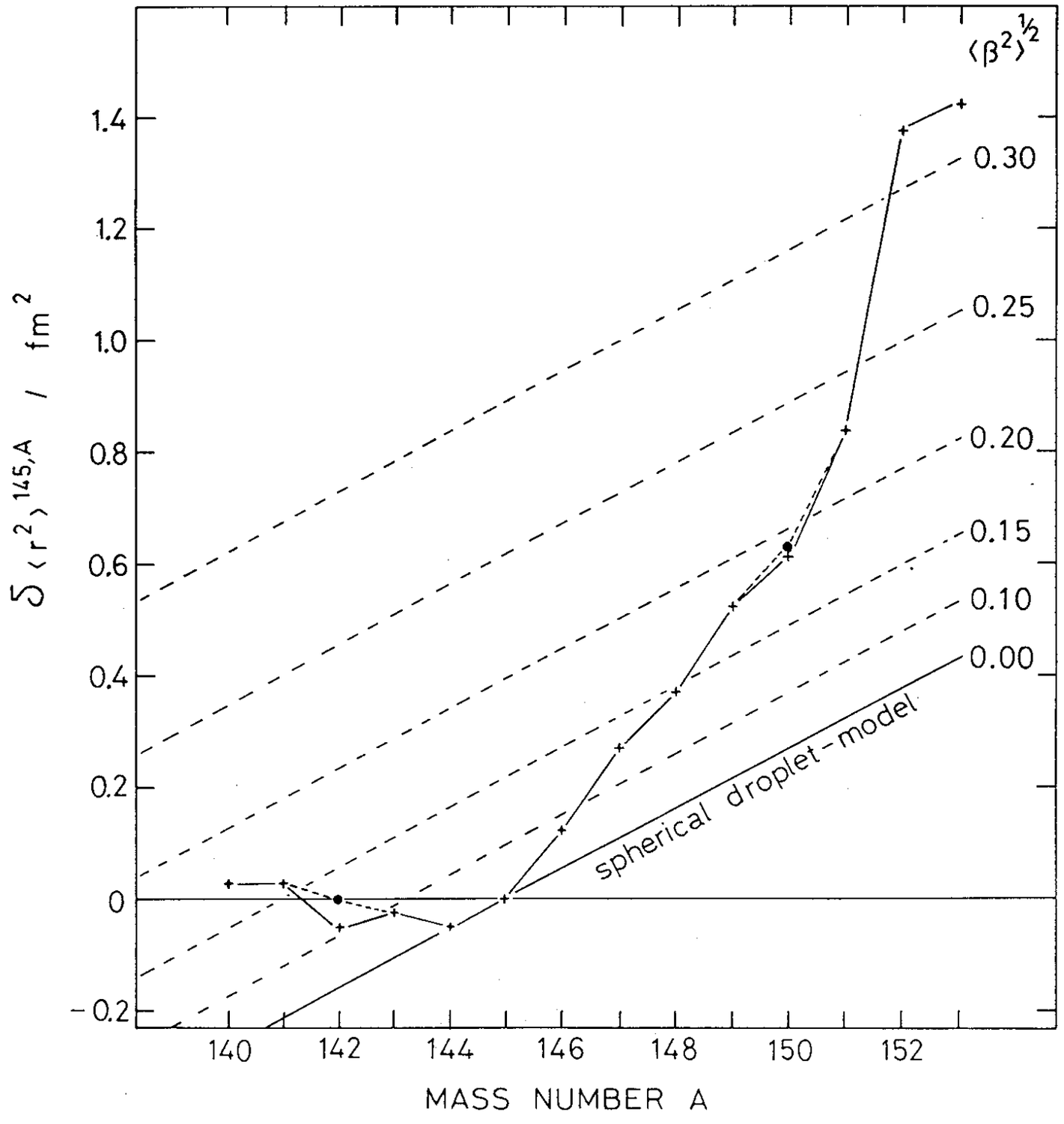
$\langle\beta^2\rangle^{1/2}$
0.30
0.25
0.20
0.15
0.10
0.00
spherical droplet-model
$\delta\langle r^2\rangle^{145,A}$ / fm^2
1.4
1.2
1.0
0.8
0.6
0.4
0.2
0
−0.2
140
142
144
146
148
150
152
MASS NUMBER A

Fig. 15

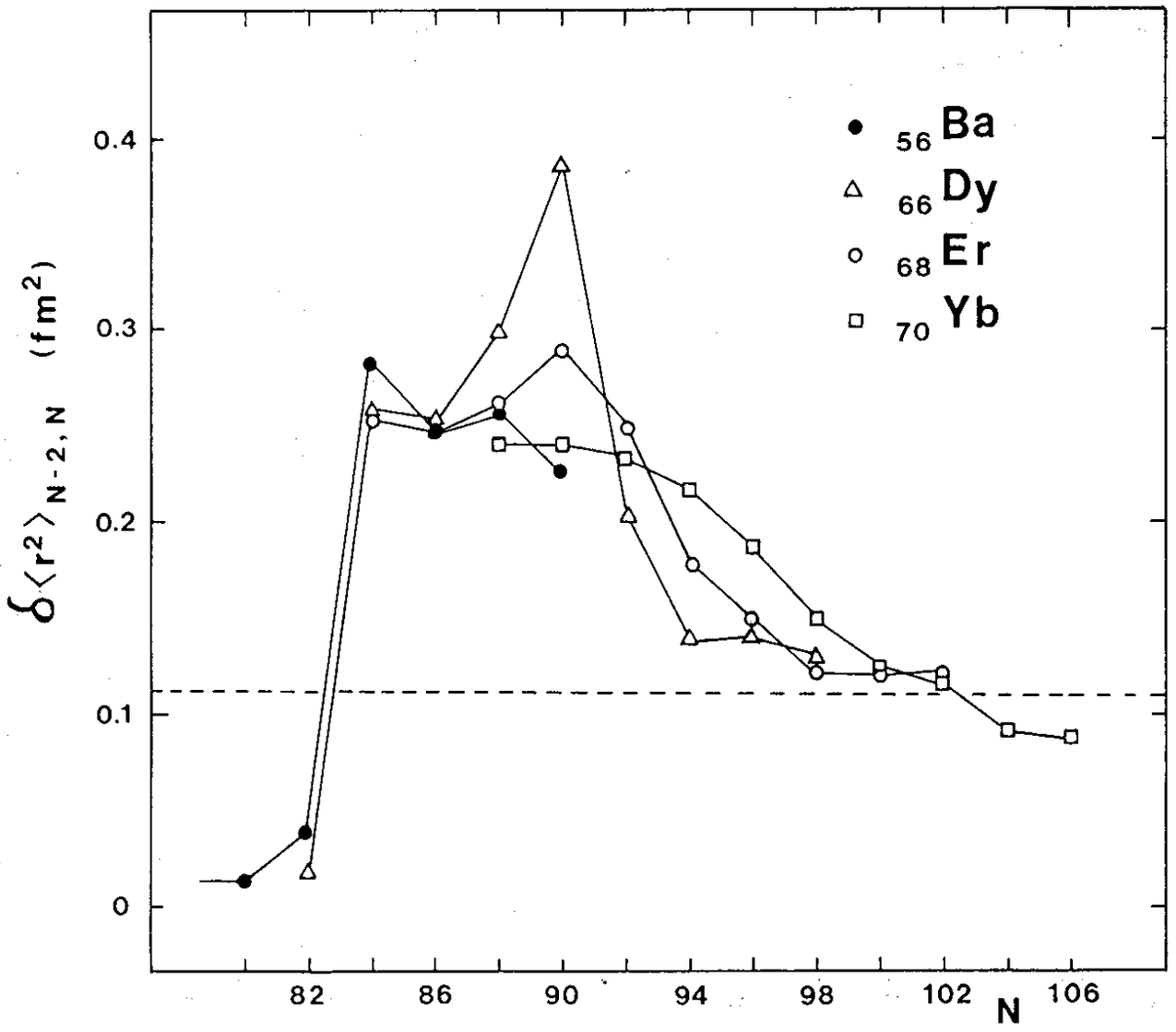
0.4
0.3
0.2
0.1
0
$\delta\langle r^2\rangle_{N-2,N}$ (fm^2)
82
86
90
94
98
102
106
N
$_{56}$Ba
$_{66}$Dy
$_{68}$Er
$_{70}$Yb

Fig. 16

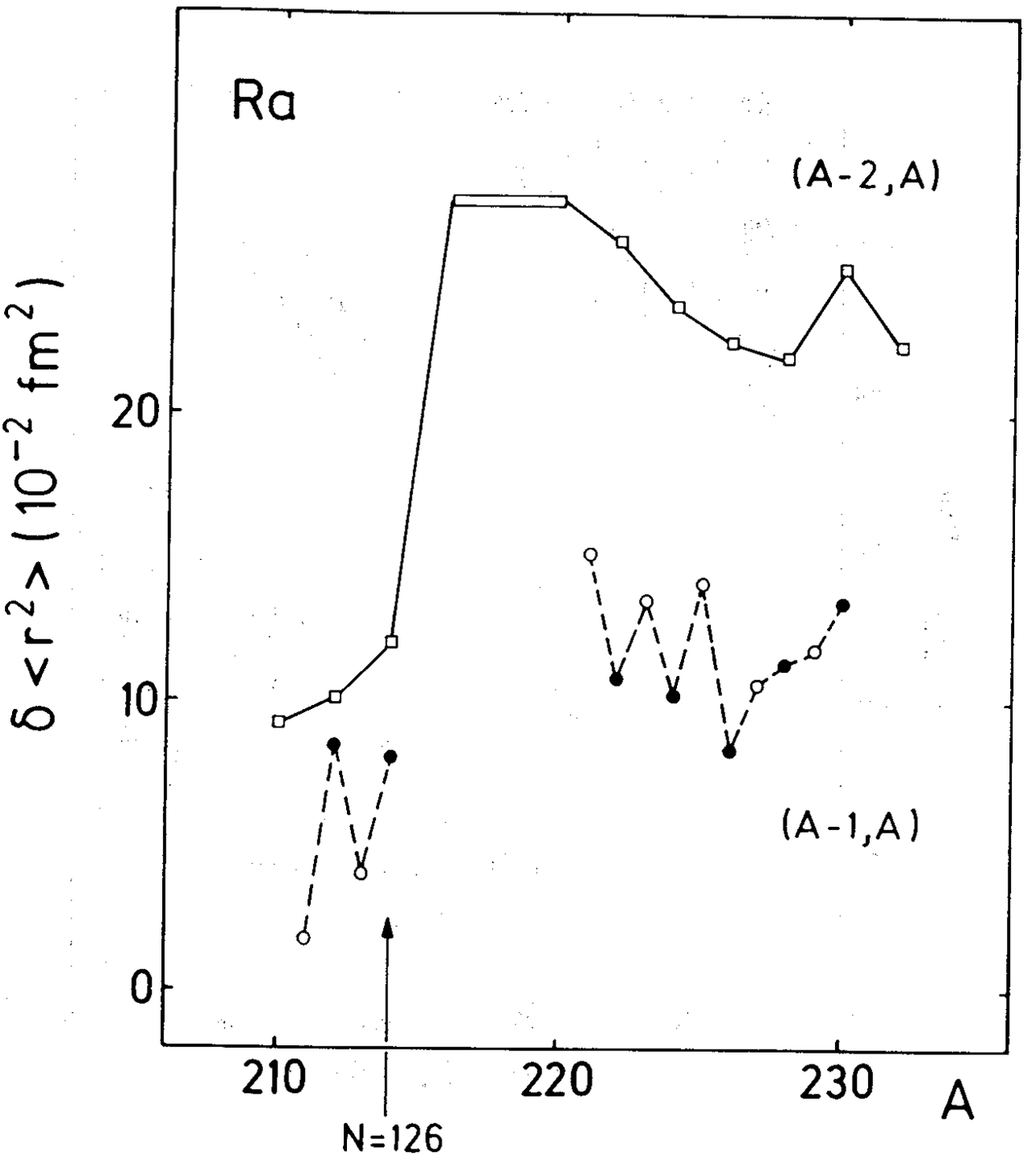
Ra
(A-2,A)
(A-1,A)
$\delta \langle r^2 \rangle$ (10^{-2} fm^2)
20
10
0
210
220
230
A
N=126

Fig. 17

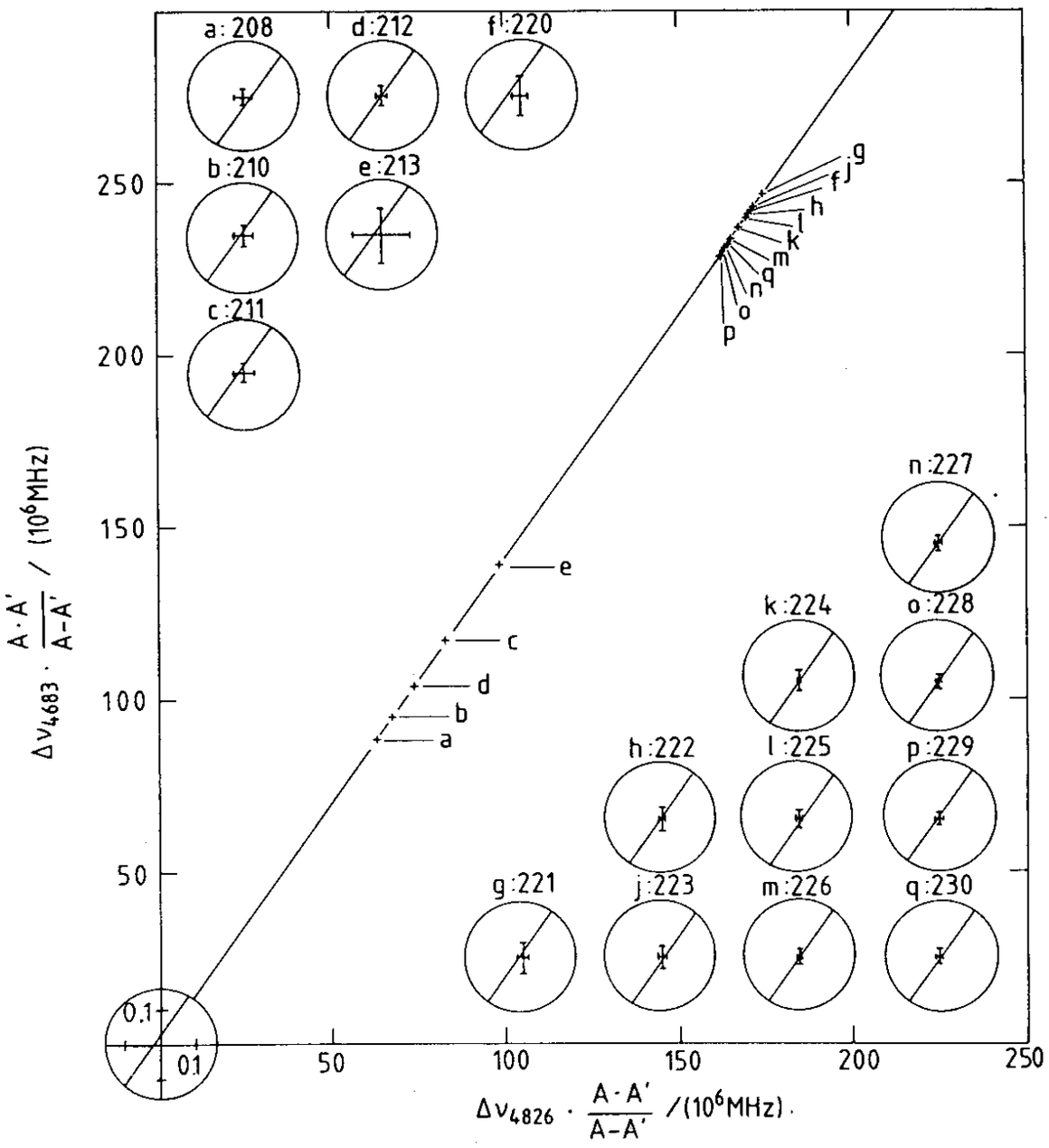
a: 208
d: 212
f: 220
b: 210
e: 213
c: 211
g
f
j
h
l
k
m
q
n
o
p
n: 227
k: 224
o: 228
h: 222
l: 225
p: 229
g: 221
j: 223
m: 226
q: 230
e
c
d
b
a
0.1
0.1
50
100
150
200
250
50
100
150
200
250
$\Delta\nu_{4683} \cdot \frac{A \cdot A'}{A - A'}$ / (10^6MHz)
$\Delta\nu_{4826} \cdot \frac{A - A'}{A - A'}$ /(10^6MHz).

Fig. 18

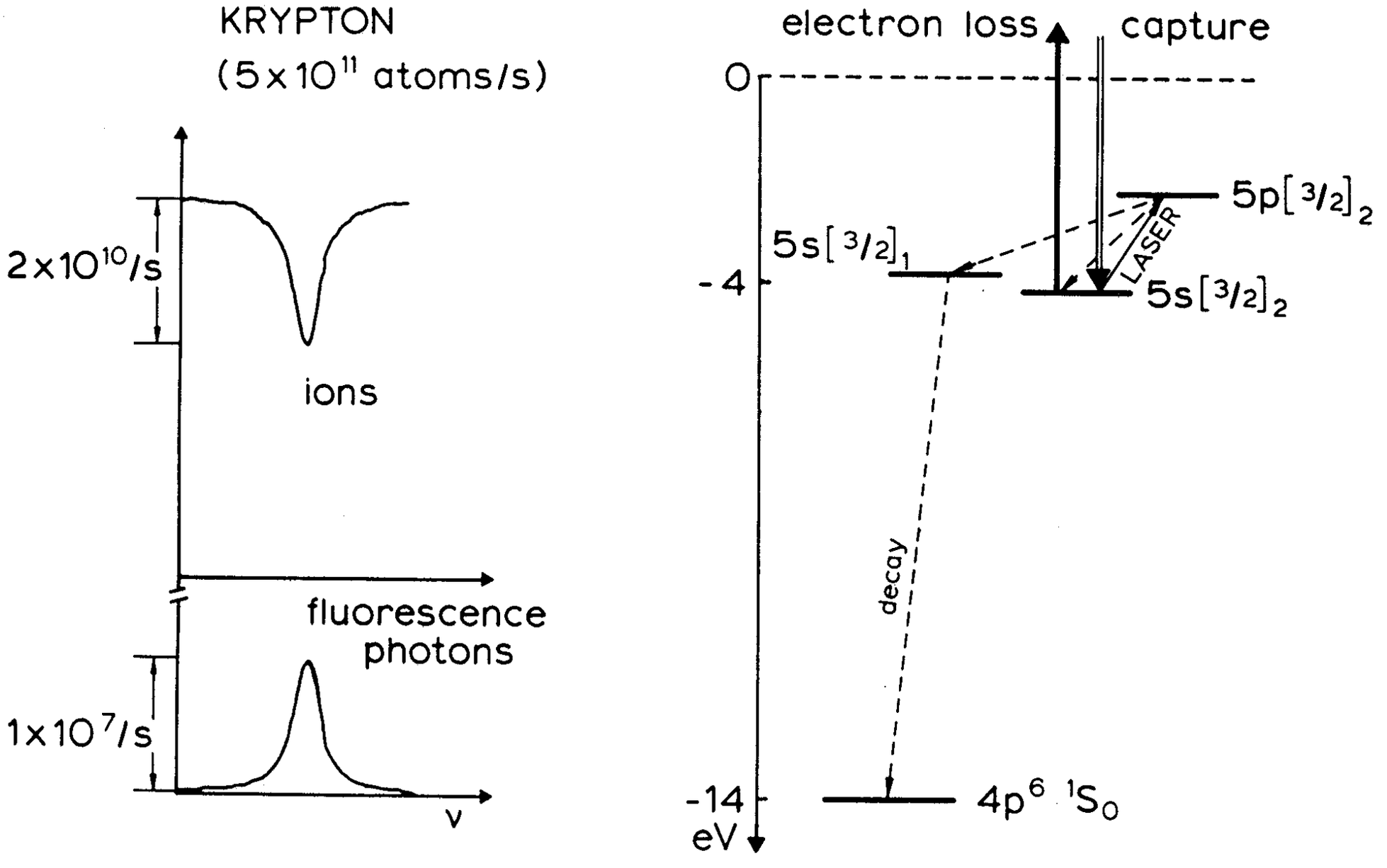
KRYPTON
(5x10^11 atoms/s)
2x10^10/s
ions
fluorescence
photons
1x10^7/s
ν
electron loss
capture
0
-4
-14
eV
5p[3/2]2
5s[3/2]1
5s[3/2]2
LASER
decay
4p^6 1S0

Fig. 19